









# Interactions between tectonics, bedrock inheritance and geomorphic responses of rivers in a post-rifting upland (Ponta Grossa Arch region, Brazil)

Marcilene dos Santos<sup>1\*</sup> , Francisco Sergio Bernardes Ladeira<sup>2</sup> , Alessandro Batezelli<sup>2</sup> , João Osvaldo Rodrigues Nunes<sup>3</sup> , Eduardo Salamuni<sup>4</sup> , Clauzionor Lima da Silva<sup>5</sup> , Eder Cassola Molina<sup>6</sup> , Isabel Cristina Moraes<sup>7</sup> 

## Abstract

Tectonic rejuvenation has been widely described in ancient rifting areas of intraplate settings, despite extensive active tectonics being discontinued long ago. Various models have been invoked to justify such tectonic rejuvenation, suggesting that the long-term deformation in intraplate interiors may be more complex than once supposed. Inherited weakness zones, e.g., pre-existing faults are stress concentrators. However, not all weakness zones in plate interiors show tectonic rejuvenation and recognizing intraplate fault reactivation remains puzzling. Bedrock channels play an essential role in tectonically unstable landscapes and therefore they may unveil which pre-existing structures have been rejuvenated. Here we explore the Cinzas Catchment in order to investigate the interactions between tectonic rejuvenation, bedrock inheritance and geomorphic river signatures in an important Brazilian rifting feature, the Ponta Grossa Arch. We perform a geomorphic analysis combined with fieldwork, dating techniques and existing data to evaluate whether the geomorphic responses of the major rivers show perturbations related to the bedrock inheritance and post-rift rejuvenation. We also show that the interactions between river signatures and the bedrock fault zones are responses to post-rifting rejuvenation coupled with bedrock inheritance. This post-rifting rejuvenation is consistent with a mosaic of superimposed mechanisms which have been invoked by previous studies.

**KEYWORDS:** geomorphic analysis; bedrock inheritance; post-rifting tectonics; tectonic rejuvenation; Quaternary.

## INTRODUCTION

In post-orogenic landscapes of continental intraplate settings, where extensive active tectonics ceased tens to hundreds of millions of years ago, a range of driving mechanisms has been invoked to explain their usual Neogene tectonic rejuvenation

(Bishop 2007, Gallen and Thigpen 2018). Therefore, whether episodic or continuous, such tectonic rejuvenation has been justified as a result of:

- denudational isostatic rebound (e.g., Baldwin *et al.* 2003, Bishop and Goldrick 2010);
- far-field stress from far plate tectonic sources such as spreading ridge or orogen pushes (e.g., Cobbold *et al.* 2001, Cogné *et al.* 2013, Marques *et al.* 2013, Talwani 2014);
- differential lithospheric rheology and strength or flexural stress (e.g., Zoback and Richardson 1996, Powell and Thomas 2016);
- influence of pre-existing crustal weakness (e.g., Silva and Sacek 2019);
- variability and contrasting lithological strength (e.g., Bishop and Goldrick 2010, Gallen 2018, Peifer *et al.* 2021);
- a combined mosaic of superimposed mechanisms (e.g., Silva and Sacek 2019, Marques *et al.* 2021).

This variety of models suggests that the long-term deformation along intraplate interiors may be more complex than once supposed (Stein and Mazzotti 2007, Gallen and Thigpen 2018).

Ancient rift structures and boundaries of cratons with adjacent lithospheric blocks with different strengths, which are common in post-orogenic regions, are likely the most substantial intraplate stress concentrators (Mooney *et al.* 2012, Talwani 2014, 2017). In addition, modelling from thermo-mechanical numerical experiments suggests that pre-existing

### Supplementary data

Supplementary data associated with this article can be found in the online version: [Supplementary Table A1](#) and [Supplementary Figures A1 and A2](#).

<sup>1</sup>Universidade Estadual Paulista “Júlio de Mesquita Filho” – Ourinhos (SP), Brazil. E-mail: marcilene.santos@unesp.br

<sup>2</sup>Universidade de Campinas – Campinas (SP), Brazil. E-mails: ladeira@unicamp.br, batezeli@unicamp.br

<sup>3</sup>Universidade Estadual Paulista “Júlio de Mesquita Filho” – Presidente Prudente (SP), Brazil. E-mail: joao.o.nunes@unesp.br

<sup>4</sup>Universidade Federal do Paraná – Curitiba (PR), Brazil. E-mail: salamuni@ufpr.br

<sup>5</sup>Universidade Federal Rural do Rio de Janeiro – Rio de Janeiro (RJ), Brazil. E-mail: clauzionor@ufrj.br

<sup>6</sup>Instituto de Astronomia, Geofísica e Ciências Atmosféricas, Universidade de São Paulo – São Paulo (SP), Brazil. E-mail: eder.molina@iag.usp.br

<sup>7</sup>Universidade Federal do Recôncavo da Bahia – Cruz das Almas (BA), Brazil. E-mail: isabelmoraes@ufrb.edu.br

\*Corresponding author.



weakness zones (e.g., major faults and Precambrian shear zones) coupled with differential denudation play a substantial role for stress/strain concentration and tectonic rejuvenation in the continental interiors of decoupled and hyperextended lithosphere settings (e.g., the post-rift Brazilian margin in Southeastern/Southern Brazil) (Silva and Sacek 2019, Silva 2021). However, not all inherited weakness zones in continental plate interiors show tectonic rejuvenation (Liu *et al.* 2011, Assumpção *et al.* 2014), and explaining the distribution and occurrence of intraplate faults reactivation remains puzzling (Talwani 2017, Gallen and Thigpen 2018). The reasons behind such an enigma include the fault behaviour in low tectonic strain settings that usually occurs episodically on both the temporal and spatial scale (Crone *et al.* 2003, Liu *et al.* 2011). In addition, the absence of neotectonic fault exposures may make it difficult to determine which ones are the rejuvenated sectors of landscapes (Quigley *et al.* 2007).

Bedrock trunk channels are considered the 'backbone' of the landscape since they set much of the relief architecture of tectonically unsteady landscapes (Whipple and Tucker 1999, Bishop and Goldrick 2010). Thus, longitudinal profiles of bedrock channels provide proxies for a variety of perturbations (e.g., Beeson and McCoy 2020), and they may unveil which pre-existing structures have been potentially rejuvenated in post-orogenic regions (Wobus *et al.* 2006, Quigley *et al.* 2007, Schwanghart and Scherler 2020).

In Southeastern/Southern Brazil, important rifting tectonics associated with the Mesozoic South Atlantic Opening were superimposed over both the Brazilian orogenic bedrock and Palaeozoic to Mesozoic sequence of the Paraná Basin. An extensive body of geologic data, including the regional stress field, geophysical sections, surface and subsurface stratigraphy (e.g., Sztamari and Milani 1999, Heilbron *et al.* 2000, Mohriak *et al.* 2008, Torsvik *et al.* 2009, Moulin *et al.* 2010), delineates the history of such rifting tectonics. In addition, post-rift tectonic reactivations (Upper Cretaceous-Quaternary) along pre-Cenozoic structures have also been described in the literature (e.g., Ferreira *et al.* 1981, Riccomini and Assumpção 1999, Cobbold *et al.* 2001, Tello Saenz *et al.* 2003, Salamuni *et al.* 2003, Strugale *et al.* 2007, Cogné *et al.* 2012, Franco-Magalhães *et al.* 2014, Santos J.M. *et al.* 2019, Silva and Sacek 2019, Marques *et al.* 2021). It is reasonable to consider that fluvial morphology/morphometry can be affected by external forces, whether combined with internal forces or not (Gailleton *et al.* 2021). However, little is known about the influence of such post-rift tectonic rejuvenation on the major rivers of the regional area.

Amongst the major structures in Southeastern/Southern Brazil associated with the Mesozoic rifting, we may highlight the Ponta Grossa Arch (PGA) as an important tectonic and magmatic feature. Four deep lineaments mainly associated with large rivers, as well as magnetic and gravimetric anomalies (Ferreira 1982, Zalán *et al.* 1991), cross and delineate the PGA (Fig. 1). Despite the substantial intraplate stress concentrators in the PGA setting, such as rift structures and craton boundaries, and the evidence of post-rift tectonic rejuvenation,

studies regarding their influence on the fluvial morphology/morphometry are still scarce.

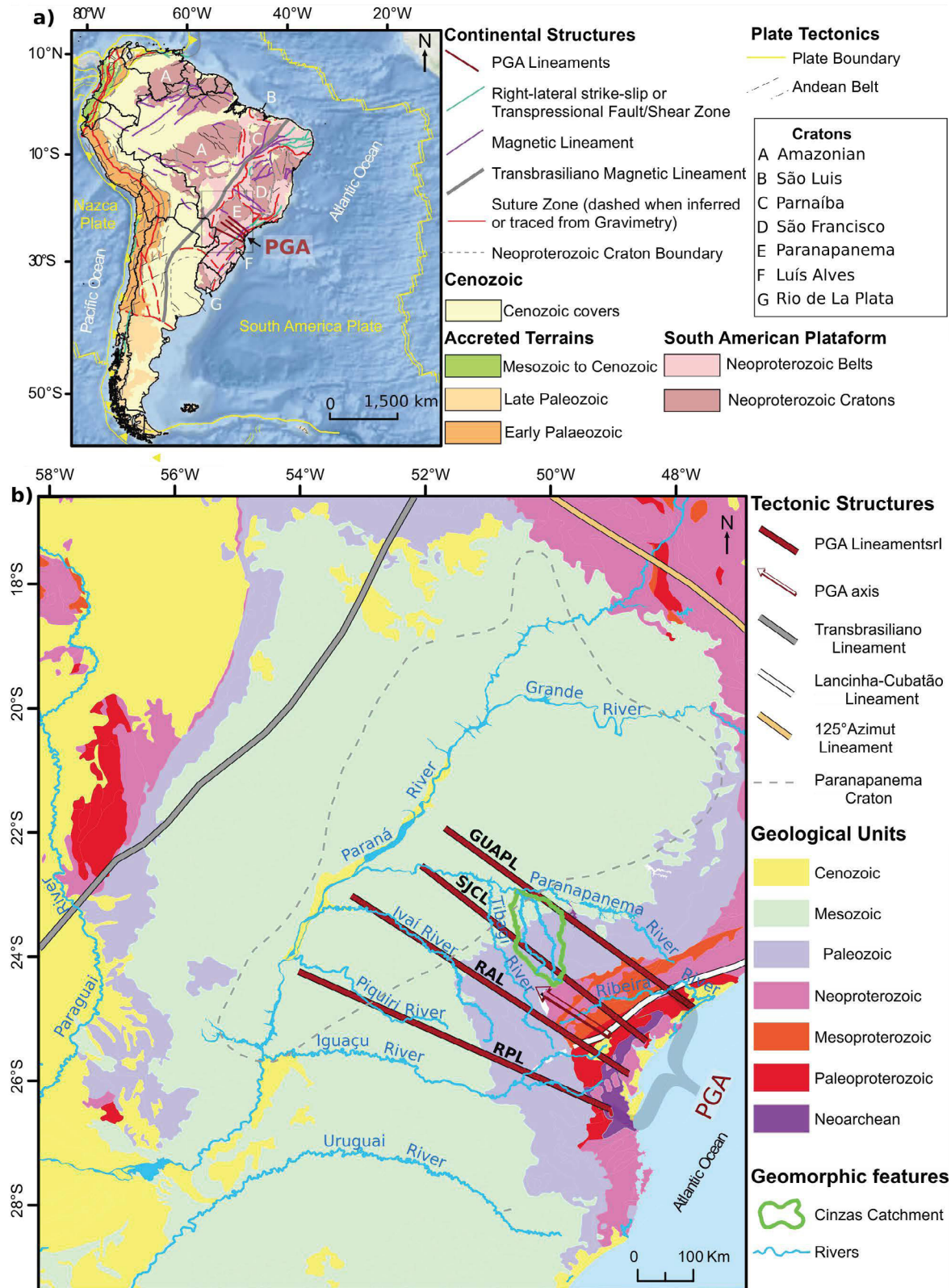
In order to contribute to closing of this gap, we focus on anomalous behaviours of the major rivers and their interplay with the Pre-Cenozoic bedrock and potential post-rift tectonic reactivations. Here we perform a quantitative and qualitative geomorphic analysis integrated with fieldwork and structural analysis, gravity and aeromagnetic data, open access geological maps and dating techniques, supported by imagery analysis and DEM-SRTM models. We examine this issue in the context of the Cinzas catchment, a large river basin located on the eastern edge of the PGA and affected by one of the four major lineaments and by expressive pre-rifting NE-SW-trending fault zones (Zalán *et al.* 1991, Artur and Soares 2002). We explore whether the longitudinal profiles, channel pattern of the bedrock trunk channel and the major tributaries show perturbations related to the bedrock boundaries and major pre-existing lineaments/fault zones. In addition, we also investigate signals of fault rejuvenation and potential associated sedimentary deposits.

## GEOLOGICAL SETTING

The study area is located in the eastern edge of the PGA (Ferreira *et al.* 1981), a Cretaceous uplift feature several hundreds of kilometres long from the Southeastern/Southern Brazilian offshore towards the Paraná River inland, associated with rifting and the resulting opening of the South Atlantic Ocean (Fig. 1A). Elevation of the PGA ranges from ~1,500 to 600 m (Franco-Magalhães *et al.* 2010).

Besides disturbing and dividing the Paraná Basin (450-65 Ma) into two sub-basins (Ferreira 1982), the PGA has been superimposed over the Neoproterozoic orogenic belts and suture zones (e.g., Bizzi *et al.* 2003), also crossing the overlaid Neoproterozoic Paranapanema Craton (e.g., Mantovani *et al.* 2005) (Fig. 1A). The PGA, delineated by four major NW-SE-trending lineaments referred to as the Guapiara, São Jerônimo-Curiúva, Rio Alonzo and Rio Piquiri (Ferreira *et al.* 1981, Ferreira 1982, Zalán *et al.* 1991) an area about ~600 km long and > 250 km wide (Fig. 1B). It is also marked by alkaline intrusions (Early to Upper Cretaceous; Riccomini *et al.* 2005, Marangoni and Mantovani 2013) and two expressive diabase dyke swarms (~130 Ma; e.g., Soares *et al.* 2016). Geophysical expression of the PGA is evidenced by remarkable magnetic and gravimetric anomalies (Ferreira *et al.* 1981, Ferreira 1982, Marangoni and Mantovani 2013).

Large rivers are roughly fitted along these lineaments and expressive bedrock shear zones (trending NE-SW and ~E-W) which were reactivated during the rifting and post-rifting tectonics throughout the PGA region (Fig. 1B). For instance, the Piquiri and Ivaí Rivers are embedded along the Piquiri and Alonzo lineaments, respectively, whereas the Ribeira and Iguaçú Rivers flow along the Lancinha-Cubatão Lineament (Fig. 1B). Previous studies have inferred fault reactivation along these weakness zones associated with post-rift tectonic events during the Upper Cretaceous, Paleogene and Neogene to Quaternary (e.g., Saadi *et al.* 2002, Tello Saenz *et al.* 2003,



GUAPL: Guapira; SJCL: São Jerônimo-Curiúva; RAL: Rio Alonso; RPL: Rio Piquiri.

Source: adapted from Riccomini *et al.* (2005) and Cordani *et al.* (2016).

**Figure 1.** Geological framework of the study area. (A) Tectonic setting of the South American Platform and the Ponta Grossa Arch (PGA). (B) Geological context of the Cinzas Catchment.

Riccomini *et al.* 2004, Hackspacher *et al.* 2007, Strugale *et al.* 2007, Salamuni *et al.* 2017, Peyerl *et al.* 2018, Santos J.M. 2019a, Silva and Sacek 2019).

Geological and thermochronological data from apatite fission-track and (U-Th)/He have registered ~4 km of total

post break-up denudation (Cobbold *et al.* 2001, Cogné *et al.* 2011) and at least three major post-rift tectonic events with high cooling and denudation rates along the PGA and its surroundings (e.g., Cobbold *et al.* 2001, Riccomini *et al.* 2004, Franco-Magalhães *et al.* 2010, Cogné *et al.* 2012):

- Late Cretaceous (from ~90 to ~65 Ma), under a strike-slip regime;
- Paleogene (from ~60 to ~25 Ma), associated with an extensional regime;
- Neogene/Quaternary (from ~15 Ma to present), under dominant strike-slip regime attributed to regional compression due to far-field stress.

The exhumation history of the PGA (e.g., Franco-Magalhães *et al.* 2010) indicates the São Jerônimo-Curiúva Lineament as a substantial post-rift stress concentration zone. For instance, the São Jerônimo-Curiúva Lineament divided the Cretaceous uplift feature into two areas with distinctive exhumation histories demonstrated by a discrepancy in age around 30 Ma between them (a NE younger portion ac. 20 Ma and one older SW ac. 50 Ma) (Suppl. Fig. A1) (Franco-Magalhães *et al.* 2010). This discrepancy was interpreted as a result of the Neogene reactivation (from Miocene onwards) and tectonic-driven differential denudation due to far-field stress from the Andean orogeny (Franco-Magalhães *et al.* 2010, 2014). This rejuvenation of the São Jerônimo-Curiúva Lineament changed the source area and the transport trending of sedimentary supply from the offshore Santos Basin from WNW to WNW/NNW (e.g., Franco-Magalhães *et al.* 2010).

Various studies in the region have improved the understanding of the tectonic reactivations during the Quaternary, pointing out to an average E-W-trending of compressive  $SH_{max}$  associated with the far-field stress (e.g., Riccomini and Assumpção 1999, Hasui *et al.* 2000, Morales *et al.* 2001, Riccomini *et al.* 2004). Furthermore, fault kinematic indicators demonstrate variation in the stress regime with time (Riccomini and Assumpção 1999, Riccomini *et al.* 2004, Salamuni *et al.* 2017). Thus, a NW-SE compressive stress field under E-W right-lateral strike-slip regime was active during the Late Pleistocene-Holocene (Riccomini and Assumpção 1999, Riccomini *et al.* 2004), followed by a WNW-ESE to NW-SE extensional  $Sh_{max}$  during the Early Holocene that later changed to a current ~E-W horizontal compressive  $Sh_{max}$  (Riccomini and Assumpção 1999, Riccomini *et al.* 2004).

Despite the short period of the seismicity documentation in Brazil (~300 years of historical record), paleoseismicity/seismicity studies show a substantial concentration of epicentres in the PGA region, mainly distributed in the offshore zone (Assumpção *et al.* 2014). In the continental area of SE Brazil, these authors argue that higher seismicity rates are associated with craton edges, rifting structures and dead orogen regions. This neotectonic framework is congruent with the results found in the South American mid-plate (e.g., Assumpção 1998, Riccomini and Assumpção 1999, Assumpção *et al.* 2014), which bears evidence to an association between major seismic zones and bedrock weakness and/or stress concentration zones by activating pre-existing faults (e.g., Ferreira *et al.* 1981, Saadi *et al.* 2002, Lopes *et al.* 2010, Vasconcelos *et al.* 2021).

This study investigated the Cinzas catchment (~9,611 km<sup>2</sup>), an NNW-SSE trending and elongated catchment located in the surroundings of the axis of the PGA (Fig. 1B). Both the trunk river and two major tributaries are bedrock channels flowing

over resistant and more erodible lithologies. Elevation ranges from 315 to 1,300 m in the Cinzas catchment, with an average elevation of 806 m.

The bedrock of the Cinzas catchment is spatially variable with contrasting lithologies, comprising of a local Neoproterozoic granite, and mainly magmatic and sedimentary rocks associated with the Palaeozoic/Mesozoic supersequences of the Paraná Basin (Milani *et al.* 2007) (Fig. 2). The units are arranged in boundaries around the Northeast trend, generally dipping towards the Northwest at low angles. The Palaeozoic sequence comprises various units mainly containing conglomerates, sandstone, siltstone, mudstone, shales and limestone. Distinctly, the Mesozoic units consist of a mix of sandstone and mainly tholeiitic effusive rocks and dykes associated with the Paraná-Etendeka event (Peate 1997). The oldest units (Devonian) are exposed around the source of the Cinzas River and give rise downward to a Permian-Carboniferous glacial sequence comprising a wide area. In contrast, the youngest ones (Jurassic/Cretaceous tholeiitic effusive) prevail throughout the lower course of the catchment (Fig. 2).

Among the four major lineaments of the PGA, the NW-SE-trending São Jerônimo-Curiúva Lineament crosses the western edge of the Cinzas catchment, which is also affected by reactivated NE-SW and ~E-W-trending bedrock shear zones (São Sebastião, Jacutinga and Guaxupé Fault Zones) (Fig. 2).

## MATERIALS AND METHODS

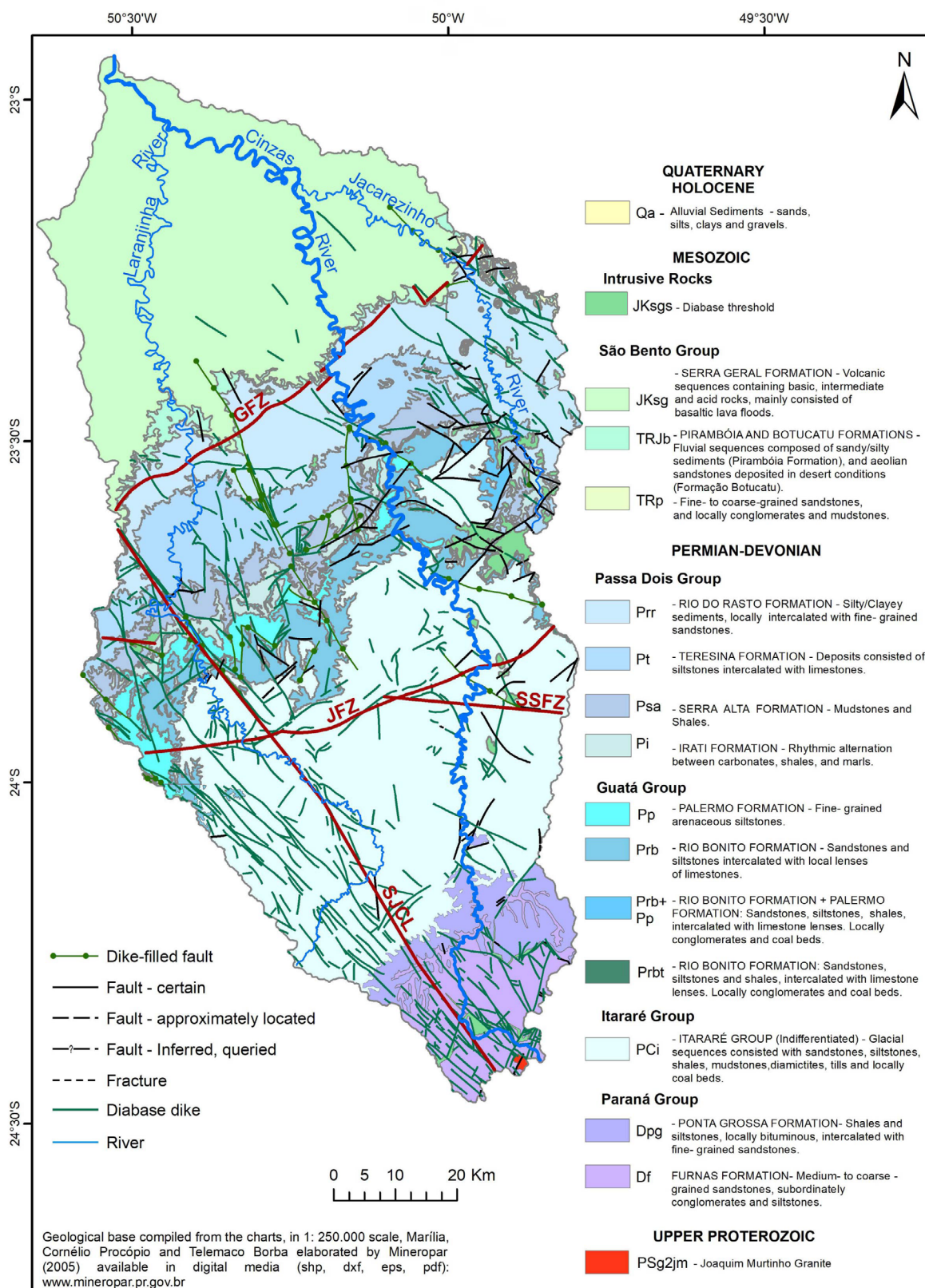
The study applied a set of techniques in order to calculate various geomorphic indicators. In addition, we performed fieldwork focused on identifying anomalies and analysing the behaviour of geomorphic signatures from major rivers in the Cinzas catchment, seeking interplays between them and the major faults as well as distinguishing those from contrasting lithology/lithological boundaries influence.

### Database

A database was built using a SRTM (Shuttle Radar Topography Mission) DEM with a spatial resolution of 30 m (<http://earthexplorer.usgs.gov/>) from the USGS Geological Survey in the GIS ArcGis 10.3 environment (ESRI 2011), Global Mapper 14 (Blue Marble Geographics/Engesat). This database consists of topographic charts in the 1:250,000 and 1:50,000 scale from the Brazilian Institute of Geography and Statistics (IBGE 1991), 1:25,000 aerial photographs available from the Institute of Land, Cartography and Geosciences (ITCG) (<http://www.geo.pr.gov.br/ms4/itcg/geo.html>). Geological mapping data of the area at 1:100,000 (published at 1:250,000) is available from the extinct Paraná Geological Service (MINEROPAR 2005), whose collection is currently held by the Instituto Água e Terra do Paraná.

### Geomorphic and tectonic analysis

First, a DEM of the study area was built from SRTM images with proper corrections and smoothing (Jenson and Domingue 1988) in order to analyse the catchment morphometric signatures. Topography- and drainage-related lineaments were



SJCL: São Jerônimo –Curiúva Lineament; GFZ: Guaxupé; JFZ: Jacutinga; SSFZ: São Sebastião. Source: modified from Zalán *et al.* (1991) and Mineropar (2005).

**Figure 2.** Geological map and major structures of the Cinzas Catchment.

extracted by manual proceedings from the DEM in conjunction with the slope map with 40% overlapping transparency to avoid the influence of false shading (Tinós *et al.* 2014). The lineaments were plotted on frequency-length rose diagrams with 10° intervals to identify the main trends, using Springer 5.1.8 (Câmara *et al.* 1996). The highlighted lineaments were

delineated as a singular main line and classified as a major or minor fault.

Gravimetric and magnetic maps of the Cinzas catchment and surroundings were used to assess the relations between geophysical anomalies, the seismoactive sectors and geological features, especially the major lineaments and faults. A third-degree

polynomial surface was removed from the Bouguer gravity anomaly data to obtain the residual Bouguer anomaly contour map for the Cinzas catchment area and surroundings.

The magnetic anomaly data from EMAG2 (Maus *et al.* 2009) was resampled from the original 2 arc min global model grid, calculated at an altitude of 4 km above the average sea level using magnetic information from marine, satellite and aeromagnetic surveys.

Swath profiles crossing the study area were generated to analyse the topography (Telbisz *et al.* 2013), using the *SwathProfiler* add-in extension for ArcGIS (Pérez-Peña *et al.* 2017). Maximum, minimum and mean topographic elevation for each swath were extracted. The enhanced transverse hypsometry index (THi\*) enabled the analysis of the hypsometric integral and dissection along the swath, considering relative local relief (Pérez-Peña *et al.* 2017).

The geomorphic assessment was based on the literature (e.g., Wobus *et al.* 2006, Burbank and Anderson 2012, Kirby and Whipple 2012, Whittaker 2012, Santos M. 2019), identifying anomalous responses from channels and catchments as well as finding influence signs of tectonic activity in the area and nontectonic factors.

The structural analysis was performed according to the different sectors of the major fault zones in the study area. The Win-Tensor software v. 9.5.1 (Delvaux and Sperner 2003) was used for the fault-kinematic analysis and tectonic stress tensor inversion (Damien Delvaux- Department of Geology — Mineralogy Royal Museum for Central Africa (Belgium) (<http://damiendelvaux.be/Tensor/WinTensor/win-tensor.html>). The Win-Tensor also provides the Frohlich diagram, which allowed us to set the studied faults according to their kinematic field and dipping.

The results of morphometric maps and geomorphic indices were correlated with geological and geomorphological data collected in the field to distinguish the lithological control and tectonic deformation influence on river responses, based on the patterns and theoretical foundations proposed in the bibliography. Chronological analysis of fluvial sediments and landslides was based on OSL dating and carried out by the Laboratório de Espectometria Gama e Luminescência (LEGaL) (IG- USP). Thus, the results presented consist of an integrated and multiscale approach of remote sensing data, topography analysis, geomorphic assessment and field surveys.

## RESULTS

### Seismicity, lineaments and major faults

Along the S/SE Brazilian continental margin, the higher seismic activity results from a set of combined factors according to the literature (e.g., Assumpção 1998, Assumpção *et al.* 2016). For instance, far-field stress, flexural effects from sediment load in large sedimentary basins, a weaker crust due to pre-existing weakness zones coupled with a decoupled and hyperextended lithosphere from the Mesozoic and denudational isostatic rebound may justify such seismicity (e.g.,

Assumpção 1998, Assumpção *et al.* 2016, Silva and Sacek 2019). As part of this context, the PGA region presents seismicity, which is characterized by earthquakes with variable magnitudes (including the historical records), ranging from 4.0-5.0 to < 1.0, mainly along the continental shelf (Fig. 3A). Despite the scarce data from focal mechanisms in the PGA region, the existing data show reverse faulting associated with S1 roughly E-W (Assumpção *et al.* 2016). For the surroundings of the Cinzas catchment, the records show earthquakes over time. Recent seismic activity (in 2019 and 2018) has occurred along the Cinzas River's source with magnitudes between 2.0 and 3.0, as well as in the lower course of the Tibagi catchment (the adjacent catchment in the western boundary) (Fig. 3).

The residual Bouguer anomaly map highlights NW-SE and NE-SW trends delineated by a framework of elongated high and low anomalies (Fig. 3B). The prominent feature is characterized by a set of NW-SE elongated high anomalies affecting the southwestern portion of the Cinzas catchment, which coincides with the SJCFZ and associated dykes swarm (Figs. 1 and 2). The magnetic anomaly map also presents a coincident NW-SE-trending positive anomaly along this sector (Fig. 3C) and enhances the results from the literature (e.g., Ferreira 1982, Strugale *et al.* 2007). However, two NE-SW-trending positive magnetic anomalies are prevalent in the Cinzas catchment (Fig. 3C). The JFZ coincides with the boundary between the high and low residual Bouguer (Figs. 3A and 3B), as well as the magnetic anomalies in the middle course of the Cinzas catchment (Figs. 3A and 3C). Furthermore, the GFZ matches the southern edge of the major NE-SW-trending high magnetic anomaly, which is associated with the volcanic sequences of the Serra Geral Formation (Figs 2, 3A and 3C).

The structural lineament analysis for the study area highlights the NW-SE, NE-SW and E-W trends as preferential directions, among which the NE-SW trend comprises the most important class in both length and frequency (Fig. 4).

The NE-SW trend is comprised mainly of short segments that occur widely spread in the catchment as a whole and delineates concentrated swarms along both the GFZ and JFZ, as well as around the CMF and the upper course of the Cinzas catchment (Fig. 4). The field data indicate that this direction is associated with strike-slip faults in bedrock outcrops (both the left-lateral and right-lateral slip sense are common) and eventual normal faults, usually filled by minerals. This direction is parallel to magnetic anomalies associated with GFZ and JFZ (Figs. 3C and 4B).

It is noted that the NW-SE trend shows a wide range of directions, from N10W to N70W, prevailing the N40-50W direction as presented in the rose diagrams. The NW-SE-trending segments occur as swarms outlined by concentrated traces along similar trends that control the drainage and relief alignments, influencing both the Palaeozoic and Mesozoic lithological boundaries. Moreover, the longer segments along this direction are coincident with dykes/dyke-filled faults and both the SJCFZ and Jacarezinho valley (Figs. 2 and 4).

Field data evidence mainly left-lateral strike-slip faults with mineral filling along the NW-SE lineaments, affecting both

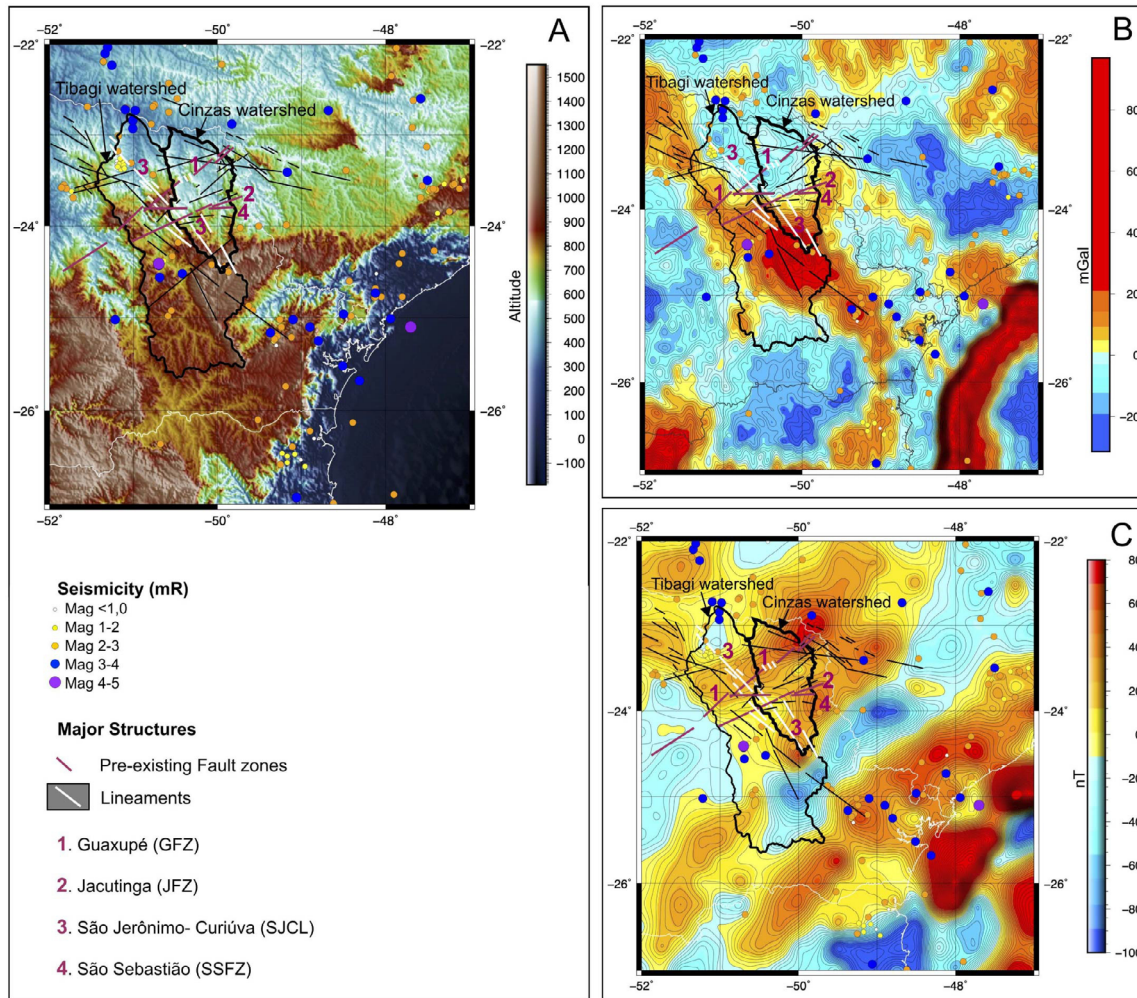


**Figure 3.** Seismicity and regional geophysical data of the Cinzas catchment area and surroundings. (A) Seismic activity in the Ponta Grossa Arch region; compiled data from the Brazilian Earthquake Catalogue, available at [www.sismo.iag.usp.br](http://www.sismo.iag.usp.br) (Bianchi *et al.* 2018). (B) residual Bouguer anomaly map with a bidimensional 3rd degree polynomial surface removed as regional and 2 mGal contour interval; (C) Magnetic anomaly map.

the Palaeozoic and Mesozoic bedrocks, and locally associated with extensional features, such as negative flower structures in basalts from the Serra Geral Formation.

Parallel to the São Sebastião Fault – SSF (Fig. 4B), the E-W segments are the third-most representative class in the Cinzas catchment, as shown in the rose diagrams (Fig. 4C). The upper course of the Laranjinha river is affected by E-W trending segments which configure three parallel lineament swarms. During fieldwork, these lineaments are associated with strike-slip faults affecting the Palaeozoic and Mesozoic bedrock, as also observed in both the NW-SE and NE-SW trends.

#### Fault kinematics and paleostress analysis

We identify 123 faults in the Cinzas Catchment, ranging from NE-SW, NW-SE, ~N-S and ~E-W trending. Their geometry and kinematic elements (e.g., polished conjugate planes, slickensides, slickenlines and fault breccia) show a prevalence of right- and left-lateral strike-slip faults followed by normal faults (Suppl. Fig. A2).

In the SJCFZ sector, the scattered pattern of the faults indicates a typical simple shear system that reactivated the NW-SE master faults accompanied by the development of Y and R

conjugate faults around the ENE-WSW trend. The results bear evidence of the SJCFZ reactivation by a paleostress field with a sub-horizontal E-W  $SH_{max}$  ( $\sigma_1$ ;  $10/267^\circ$ ) and an NNW-SSE  $SH_{min}$  ( $\sigma_3$ ;  $22/173^\circ$ ) (Fig. 5A). In addition, the Frohlich diagram shows a cluster referred to as a strike-slip stress field with mild tendency towards a transpressional regime.

For faults along the GFZ, we observe a prevalent transtensional paleostress field with two distinctive regimes (Fig. 5B). An earlier regime with NE-SW  $SH_{max}$  ( $30/237^\circ$ ) and NW-SE  $SH_{min}$  ( $15/336^\circ$ ) as well as a later one with NW-SE  $SH_{max}$  ( $40/328^\circ$ ) and NE-SW  $SH_{min}$  ( $09/230^\circ$ ), which generated more pervasive structures in the region.

In addition to an early transpressional paleostress field with a WNW-ESE  $SH_{max}$  ( $09/110^\circ$ ) and NNE-SSW  $SH_{min}$  ( $39/013^\circ$ ), the JFZ present a later one characterized as an extensional regime with sub-vertical  $SH_{max}$  ( $65/230^\circ$ ) and NW-SE  $SH_{min}$  ( $05/331^\circ$ ) which generated ENE-WSW normal faults (Fig. 5C). The first regime presents ~E-W right-lateral strike-slip faults and NW-SE left-lateral strike-slip faults, besides secondary oblique strike-slip faults. The chronology of these regimes was determinate by intersecting relations between the different fault groups in the fieldwork.

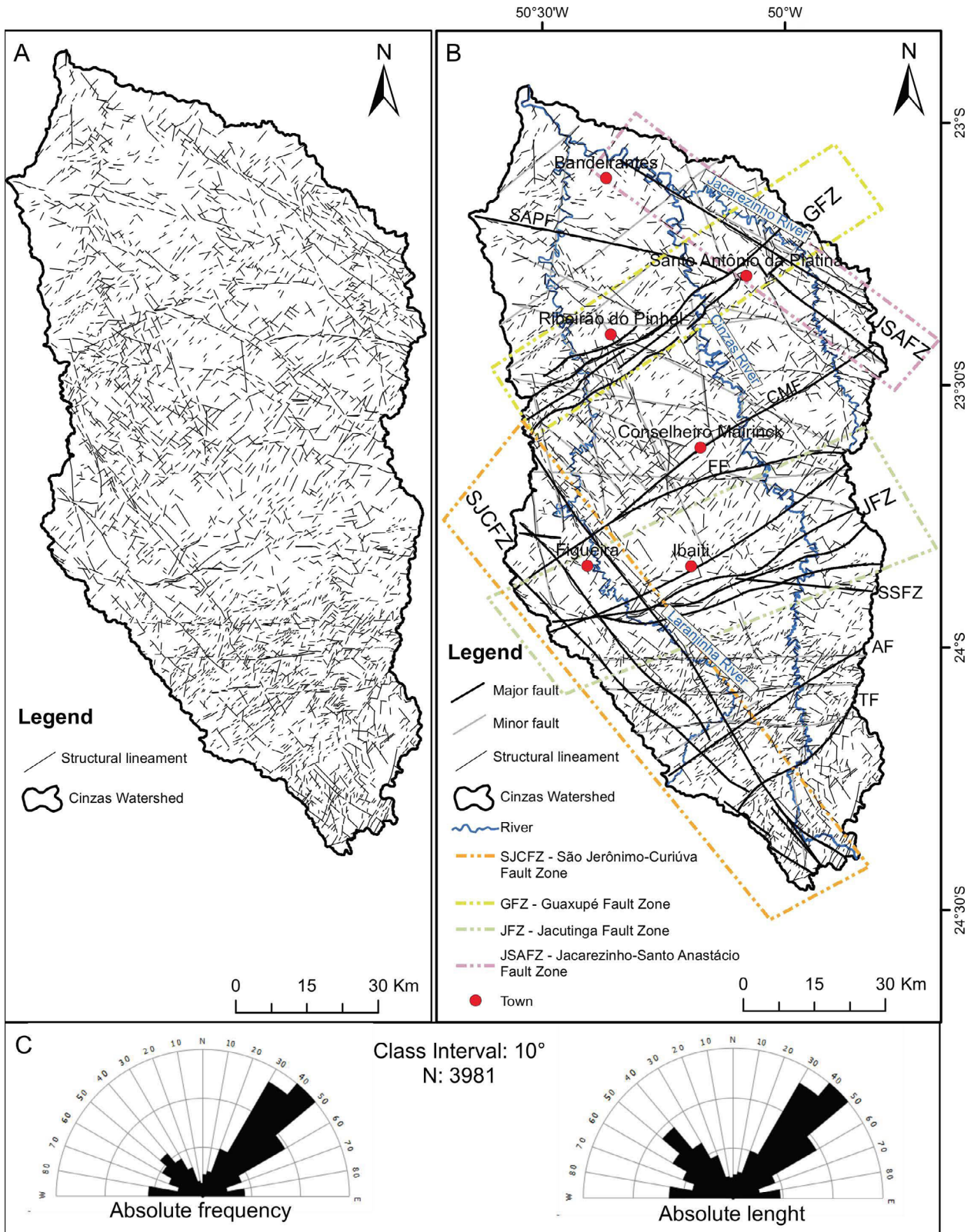


**Figure 4.** Major structures of the Cinzas Catchment. (A) Structural lineaments of the Cinzas catchment. (B) Major pre-existing fault zones and minor faults: TF – Tigre Fault; AF – Arrozal Fault; SSFZ – São Sebastião Fault Zone; FF – Figueira Fault; CMF – Conselheiro Mairink Fault; SAPF – Santo Antônio da Platina Fault. (C) Rose diagrams for lineaments of the Cinzas catchment.

We observe in the central area of the Cinzas catchment a N-S and NE-SW trending conjugate pair of strike-slip faults associated with a local NNW-SSE  $SH_{max}$  (17/334°) and NE-SW  $SH_{min}$  (14/068°) (Fig. 5D).

A conjugate pair of NNE-SSW right-lateral strike-slip and WNW-ESE left-lateral strike-slip faults occur in the JSAFZ domain in the north-eastern edge of the Cinzas Catchment,

associated with a transpressional paleostress field with NE-SW  $SH_{max}$  (16/058°) and NW-SE  $SH_{min}$  (37/160°) (Fig. 5E).

### Catchment disturbances and geomorphic responses

Table 1 summarizes the results of both the drainage basin and drainage geomorphic analysis carried out for the Cinzas



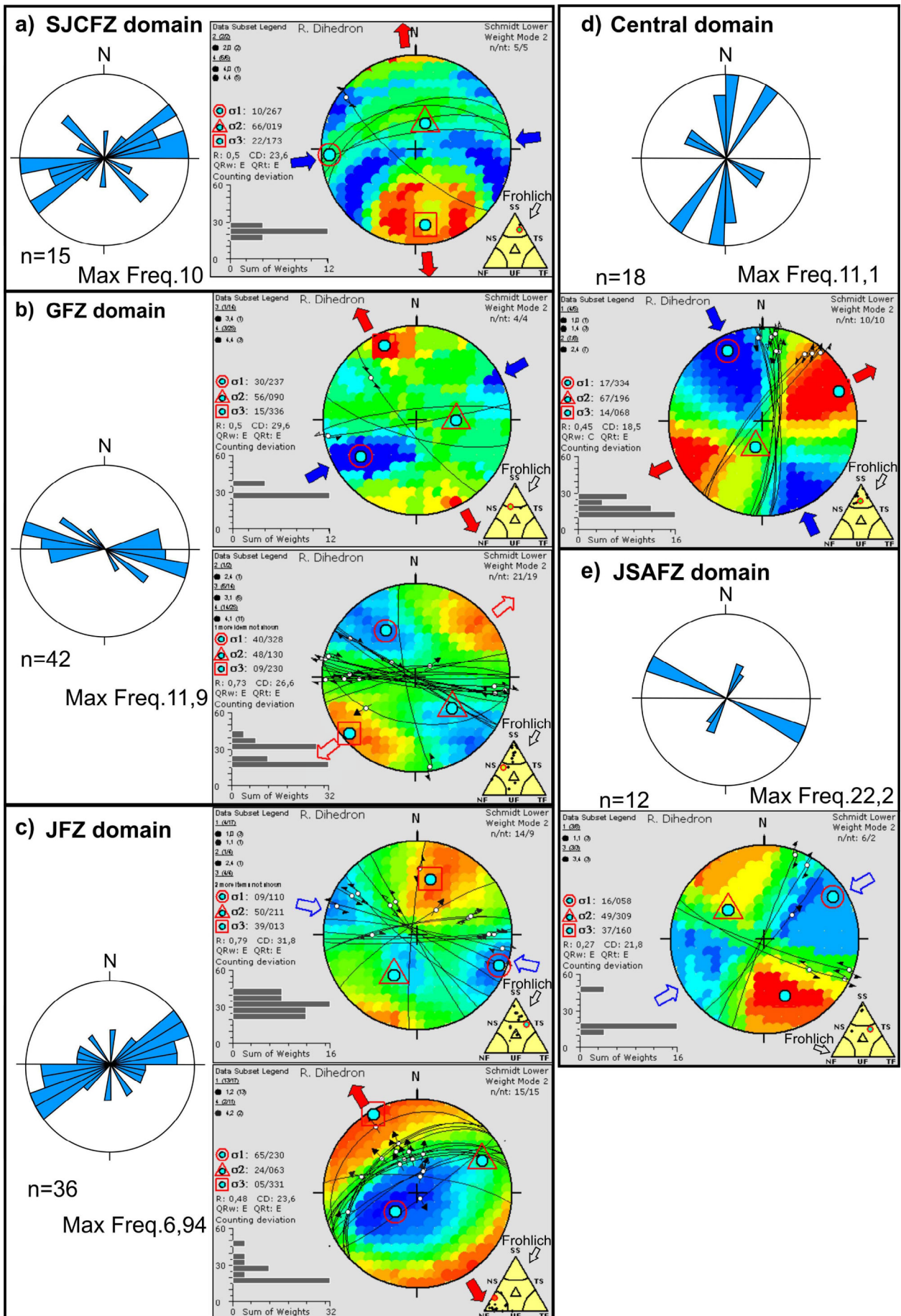


**Figure 5.** Fault kinematic and paleostress analysis in the Cinzas catchment (123 data), according to five domains; (A) SJCFZ – São Jerônimo-Curiúva Fault Zone domain, (B) GFZ – Guaxupé Fault Zone domain, (C) JFZ – Jacutinga Fault Zone domain, (D) Central domain, (E) JSAFZ – Jacarezinho-Santo Anastácio Fault Zone domain. Rose diagrams (white and blue) show the strike directions of the fault planes and the colored stereograms show traces and slip senses of faults and the paleostress tensors. Frohlich diagram (at the lower right corner) shows the stress regime.

**Table 1.** Geomorphic indices for Cinzas catchment and Laranjinha and Jacarezinho sub-basins. (For theoretical background, see Santos M. 2019).

Geomorphic Indicator	Value	Resulting Class	Determination Parameters	Analysis Standards
Basin elongation ratio ( $E_b$ )	0.31*; 0.24**; 0.26***	Elongate and tectonically active	$E_b = (\sqrt{Ab}/\pi)/L_b$ ; basin area = $\sqrt{Ab}/\pi$ ; $L_b$ = distance from the river mouth to headwater	The more elongate, the more tectonically active.
Basin shape ( $B_s$ )	2.3*; 3.5**; 3.2***	Class 1: Strong tectonic activity	$B_s = B_l/B_w$ ; $B_l$ = distance from the river mouth to headwater; $B_w$ = maximum width of a drainage basin	Levels of tectonic activity: $B_s > 2.3$ , strong (Class 1).
Drainage basin asymmetry (AF)	33.7%*; 43.8%**; 58%*** IAF-50I = -16.34*; IAF-50I = -6.2**; IAF-50I = 8.0***	Strongly tilted - Class 1*; Relatively weakly tilted - Class 3**; moderately tilted - Class 2***	$AF = 100*(A/A_s)$ ; $A_r$ = area of the basin to the right (facing downstream); $A_t$ = total area of the drainage basin	As the effect of tectonic tilting increases; IAF-50I $\geq 15$ , heavily tilted Class 1, Class 2 and Class 3.
Transverse topography symmetry (T)	Values ranges between 0.77 to 0.05*; 0.89 to 0**; 0.66 to 0***	strongly asymmetric reaches	$T = D_a/D_d$ ; $D_a$ =	the closer to $T = 1$ , the higher tectonic activity in the basin
Stream gradient index ( $SL_{seg}$ )	Values ranges between 28 to 1,003*; 43 to 706**; 25 to 153***	Strong tectonic influence and lithological control	$SL_{seg} = [(\Delta H/\Delta L)*L]$ ;	The higher $SL_{seg}$ , the stronger tectonic activity and/or the stronger hardness rock
$SL_{relativo}$ ( $SL/K$ )	Values ranges between 0.4 to 14*; 0.9 to 13.9**; 0.8 to 4.7***	Zones with high and moderate tectonic activity	$SL_{relativo} = SL_{seg}/K$	$SL_{relativo} \geq 10$ strongly anomalous; $2 \geq SL_{relativo} > 10$ anomalous; $SL_{relativo} < 2$ weakly anomalous
Sinuosity Index (P)	Values ranges between 1.2 to 2.7*; 1.1 to 2.8**; 1.5 to 2.6***	Strongly unstable sinuosity	$P = L_c/L_v$ ; $L_c$ = stream length; $L_v$ = valley length	$P = 1,0$ Straight; $1.0 < P < 1.5$ Transitional; $1.5 < P < 2.0$ Irregular; $P \geq 2.0$ Tortuous

\*Cinzas River; \*\*Laranjinha River; \*\*\*Jacarezinho River.

River and its main tributaries (Laranjinha and Jacarezinho rivers) (see Suppl. Tab. A1 for geomorphic measurement of the trunk river and its two major tributaries). The results from the drainage basin geomorphic indices, mainly the values of  $B_s$  and  $E_b$  indices, demonstrate an elongated and tectonically active character (Class 1) and high tectonic activity, as well as the T index due to its strongly asymmetric reaches (Tab. 1). It is relevant to highlight that the T anomalous values in the lower course of the drainage basins suggest tectonic forcing. Moreover, the most substantial anomaly in the upper course of the Laranjinha River fits with the sharp elbow downstream from its source (Fig. 6).

The AF index presents distinctive responses between the primary catchment and both sub-basins. For the Cinzas catchment, the AF index values present high tilting and river migration eastward. In contrast, the Jacarezinho and Laranjinha catchments present, respectively, moderate tilting and westward migration in the upper-middle course and gentle tilting as well as eastward migration. Both the SL and P indices show a wide range of values which will be presented further on.

## Channel disturbances

### Channel sinuosity

We were able to identify swaths with sudden changes of the sinuosity index and channel pattern for the Cinzas and Laranjinha rivers (Fig. 7). The tortuous pattern is prevalent, reaching the maximum possible sinuosity in a meandering river (reach 7- Laranjinha River; reach 9 — Cinzas River). In addition to the tortuous pattern, the rivers present transitional, regular and irregular patterns, except for the Jacarezinho River, where there is no transitional pattern. We observe a sharp decrease in the sinuosity index near the mouth of the Cinzas River.

Unlike the two other rivers analysed; the response from the Jacarezinho River does not present sudden changes. However, comparative analysis of sudden changes in channel patterns and sinuosity indexes for the Laranjinha and Cinzas rivers allow for delineating ENE-WSW-trending anomaly swaths (Fig. 7), as pointed out by studies of basin symmetry anomalies.

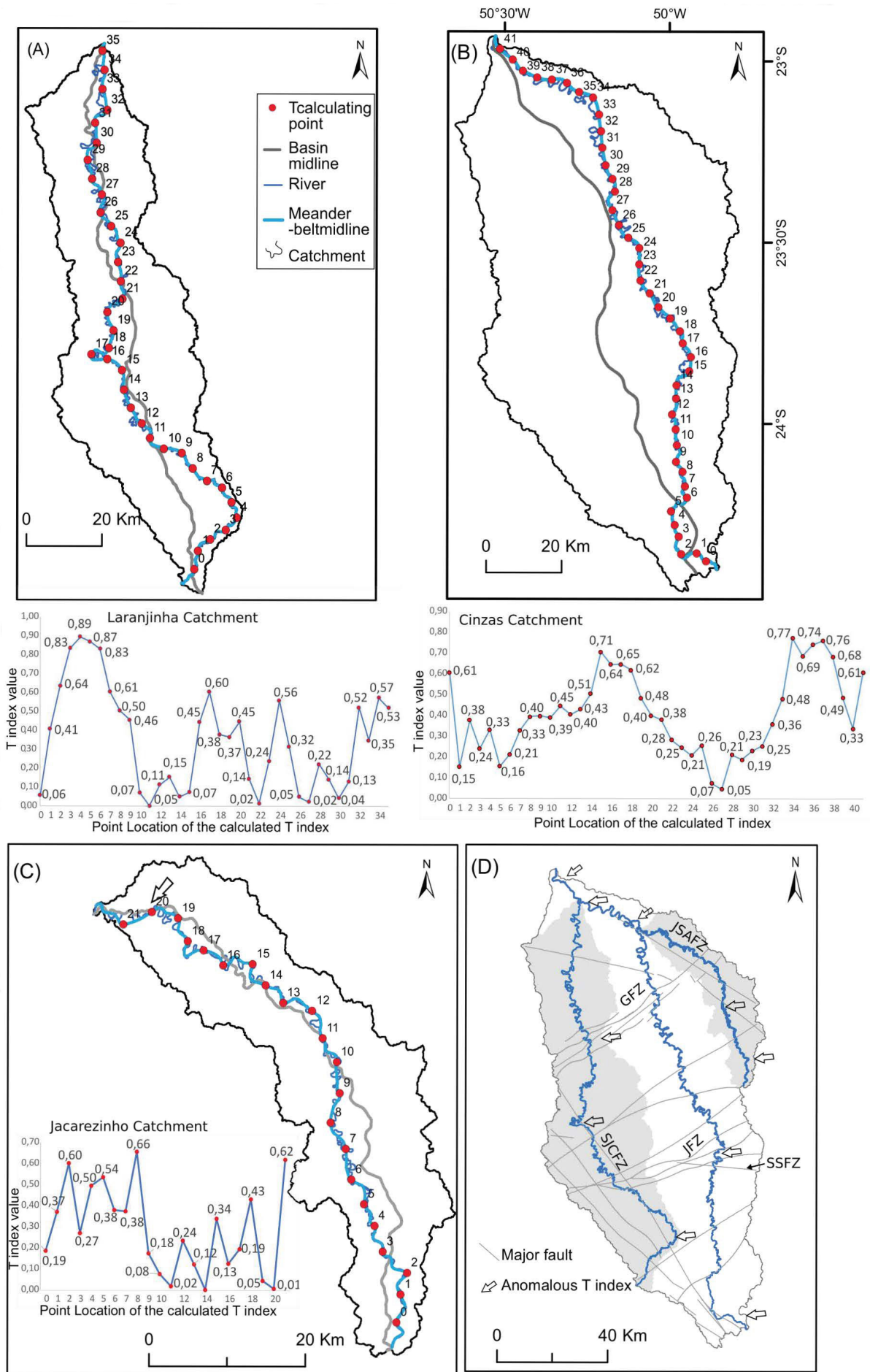


**Figure 6.** Transverse Topographic Symmetry Factor (T) for Cinzas Catchment and major sub-basins. Catchments: (A) Laranjinha, (B) Cinzas, (C) Jacarezinho; (D) T anomalous fields (arrows); red circles are the selected points for T index calculating; plots show the range of T values.

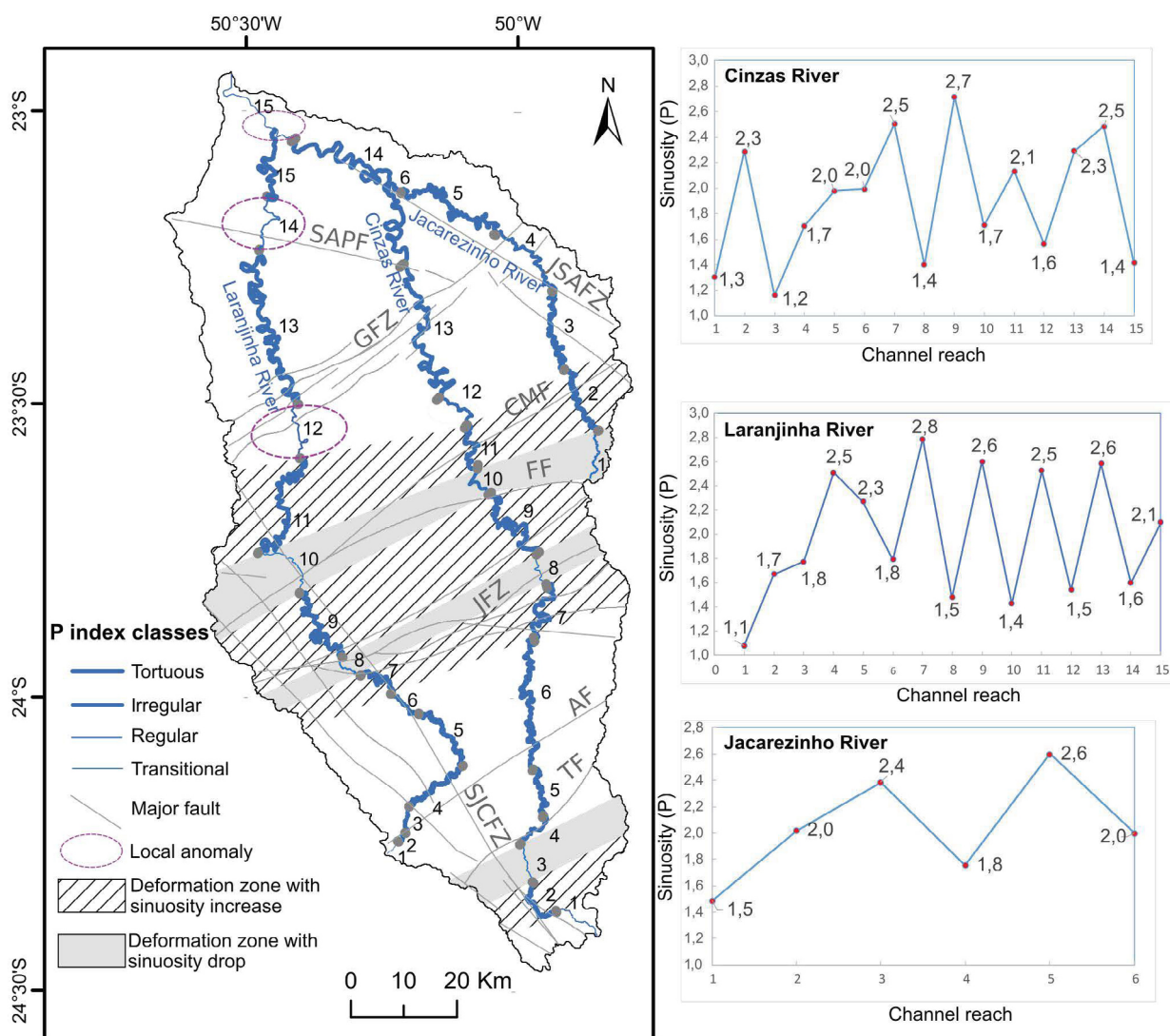


**Figure 7.** Sinuosity index and channel patterns for Cinzas catchment and major sub-basins. Plots show the P values behaviour along the Cinzas river and both the major tributaries.

**Knickpoints and channel gradient**

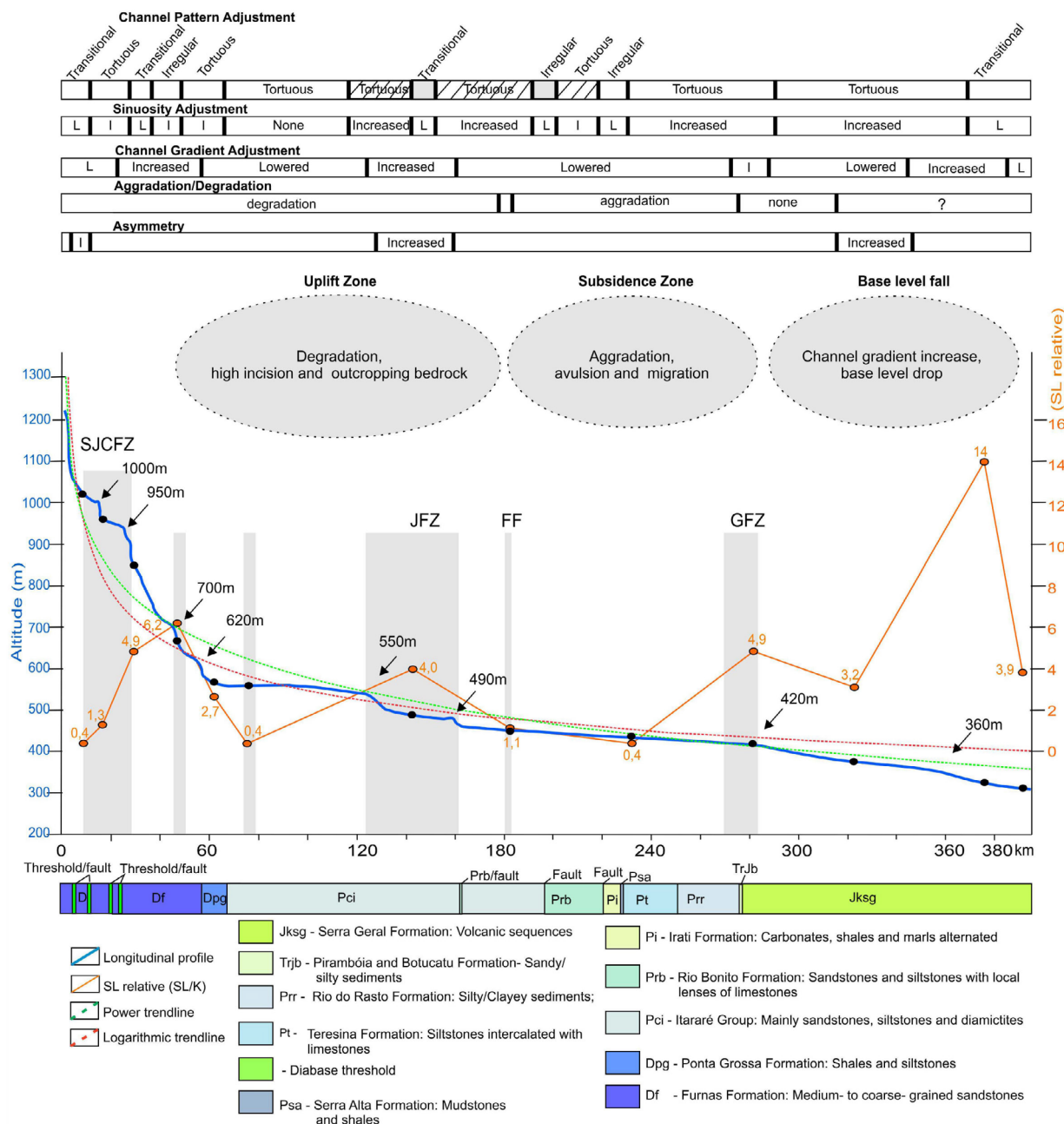
In the Cinzas catchment, numerous knickpoints occur along the major channels, mainly fitting with the major fault zones (Figs. 8 and 9). The highest knickpoints lay on elevations of 1,000 m and 900 m near the Cinzas River source, and 700 m in the upper course of the Laranjinha River, along the SJCFZ in both cases and also possibly reflecting the higher dyke strength, as well as the former catchment knickpoints (1,000 m). Nevertheless, the contrasting gradient response between the Laranjinha and Cinzas rivers along SJCFZ demands more attention, as well as the fact that these knickpoints along SJCFZ are aligned and laid on different elevations.

The knickpoints with elevations ranging from 490 m to 580 m appear to be associated with the JFZ (Figs. 8 and 9). Along the GFZ, knickpoints with elevations ranging between 500 m and 420 m mark a sharp change in the rivers which show a downward steepness/incision increase and a significant base level drop from the GFZ to the Cinzas catchment outlet, highlighting anomalous responses near the mouth of the trunk stream and its major tributaries (Figs. 8, 9 and 10A).

It is also noteworthy that a knickpoint occurs in the 360 m elevation marker, which is very close to the Laranjinha and Cinzas confluence (Figs. 8 and 10B).

The  $SL_{relative}$  index values present highly anomalous, anomalous, and lowly anomalous reaches for Cinzas and Laranjinha Rivers, while the values for the Jacarezinho River do not present highly anomalous reaches (Fig. 10A). Moreover, the most critically anomalous zone occurs in the lower course of the Cinzas and Laranjinha rivers near its mouth, distinctively from the Jacarezinho River.

We observe a clear interplay between the JFZ and GFZ and the  $SL_{relative}$  increase, which coincides with high instability in channel sinuosity as well as strong basin asymmetry, which also occurs with the SJCFZ (Figs. 8 and 9). As the GFZ fits with the Paleozoic-Mesozoic boundary of the Paraná Basin, both the GFZ and lithological strength contrasting likely influence the  $SL_{relative}$  increase. At the confluence of the Laranjinha and Cinzas Rivers, gradient values are extremely high and heavily anomalous, a sector in which the Cinzas River sharply drops in channel sinuosity. The portion of the JFZ also presents a higher incision (Fig. 10B).



SJCZFZ: São Jerônimo-Curiúva; JFZ: Jacutinga; GFZ: Guaxupé. FF: Figueira Fault.

**Figure 8.** Correlation between Cinzas River geomorphic responses and both tectonic and lithological influences. L and I mean low and increase, respectively. Black circles and arrows indicate, the selected points for SL<sub>relative</sub> index calculating and knickpoints position, respectively.

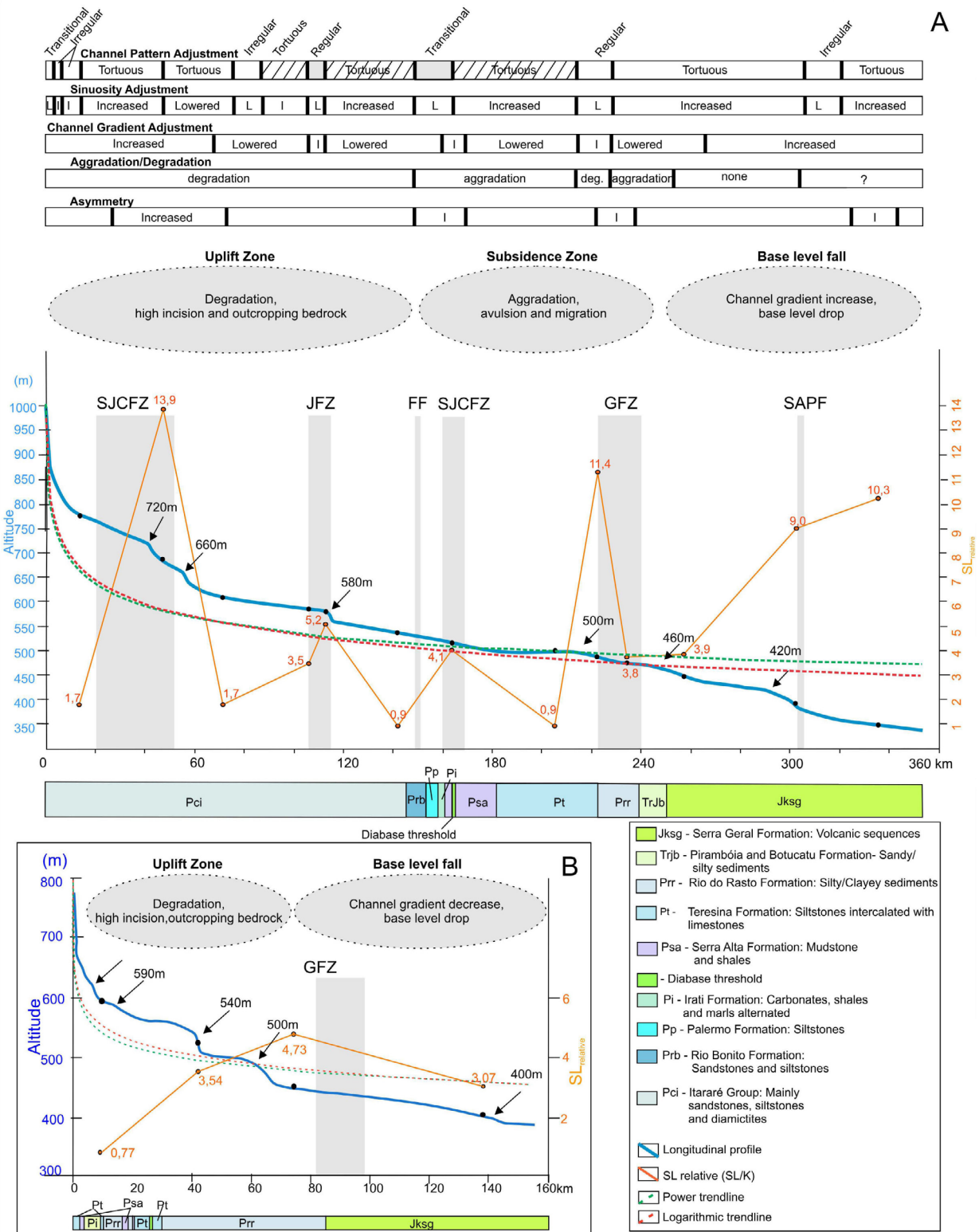
The Teresina Formation generally presents a SL<sub>relative</sub> decrease and rare knickpoints as expected due to the limestone's occurrence (cf. Seeber and Gornitz 1983), distinctively for the Itararé Group, Rio do Rasto and Serra Geral formations, where SL-relative index varies widely within their domains (Figs. 8 and 9).

Comparing the longitudinal profile of the major rivers with their best trend lines (Figs. 8 and 9), two distinct sectors are seen. One is associated with a positive anomaly that suggests an uplift in the upper course and part of the middle course. The other is prone to fit the trend lines in the medium course, which suggests a subsidence zone. Finally, a defined base-level drop combined with a high channel gradient delineates a third sector downstream the GFZ to the Cinzas catchment outlet.

**Aggradation, avulsion and migration**

Four swath profiles were carried out for topographic analysis in order to identify geomorphic surface disruptions and characterize relief dissection along the three tectonic zones pointed out from the long profiles and linked geomorphic indices of the trunk stream and major tributaries (Fig. 10). NNW-trending swath profiles 1 to 3 were set broadly orthogonal to the tectonic zones and the main NE-trending lithological boundaries, and a NE-trending swath profile (SP 4) was set parallel to the subsidence zone to analyse its geometry.

The first swath profile, SP 1, allows one to compare the along-strike variations of the Laranjinha-Cinzas divide across the tectonic zones and the main topographic features. The difference in elevation between the uplift and subsidence zones



SJCFZ: São Jerônimo-Curiúva; JFZ: Jacutinga; GFZ: Guaxupé; FF: Figueira; SAPF: Santo Antônio da Platina.

**Figure 9.** Correlation between geomorphic responses of the major (A) Laranjinha and (B) Jacarezinho rivers and both tectonic and lithological influences. L and I mean low and increase, respectively. Black circles and arrows indicate, respectively, the selected points for SL<sub>relative</sub> index calculating and knickpoints position.

is well marked (ca. 250 m in both the SP 1 and 2 and 350 m in SP 3). Moreover, the local relief is accentuated along the uplift zone and sharply decreases towards the subsidence zone, turning to high values as it hits the GFZ. At an elevation of ca. 1,000 m, a set of peaks delineates an upper surface (S1) in the uplift zone. The swath profiles highlight another surface with

elevation varying from 900 to 850 m (S2) in the uplift zone and along the GFZ and JSAFZ. Like S1, this second surface is characterized by isolated peaks, but is generally tilted towards the Northwest (Fig. 11).

The floor of the uplift zone is heterogeneous, as indicated by the curves of the mean and minimum topography, suggesting

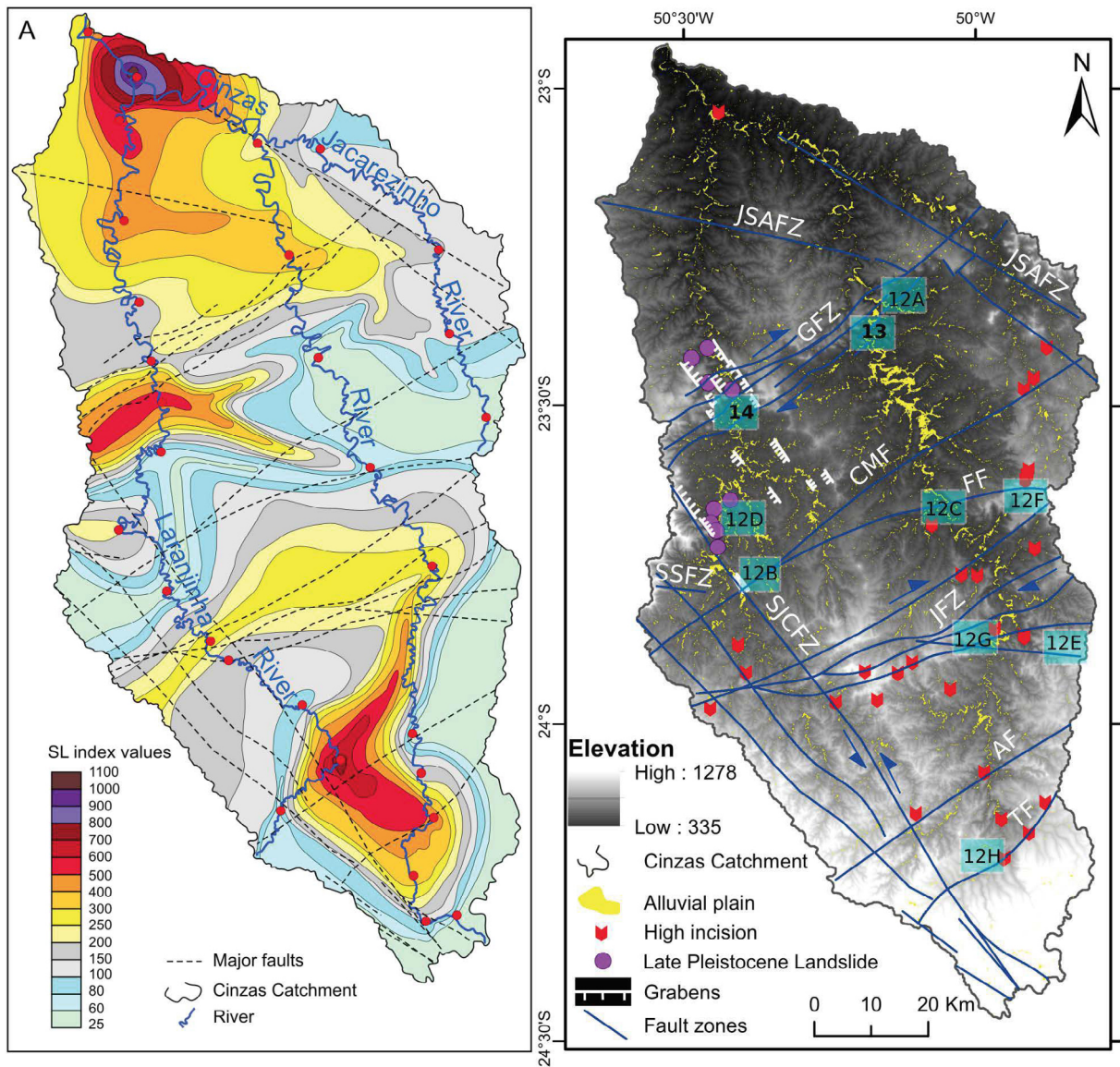


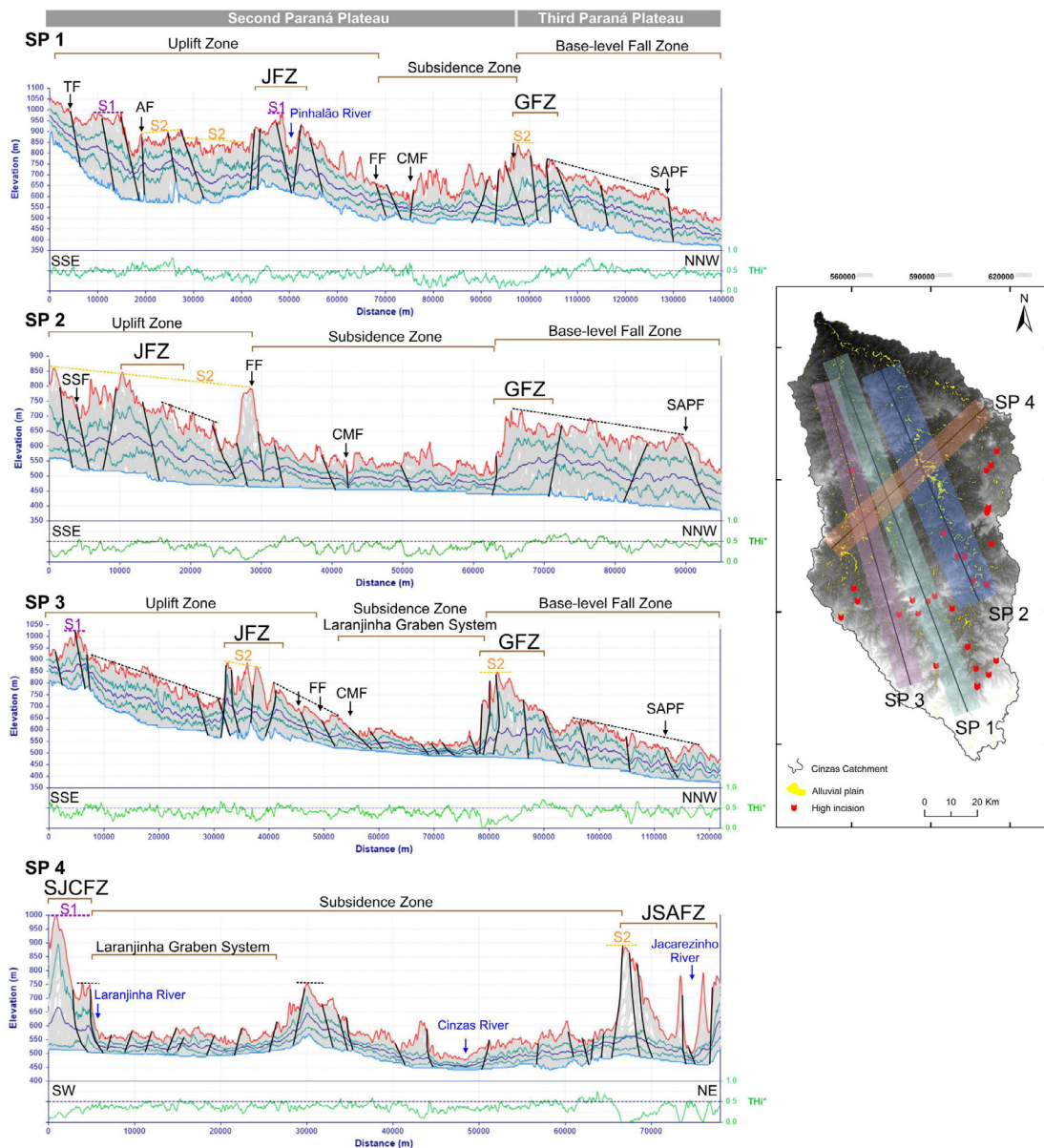
**Figure 10.** Geomorphic responses and Late Pleistocene features in the Cinzas catchment. (A) Contour map of SL index values; dashed lines represent the major faults; red circles are point locations of the measured SL index. (B) Laranjinha Graben System (white traces) and landslide clusters roughly along intersection between NW and NE fault zones; coloured polygons show the photography locations of Figure 12 and numbered 13 and 14 polygons place the Figures 13 and 14, respectively.

an association with the faults. In contrast, the floor of the subsidence zone tends to present a flat topography, appearing as three blocks tilted towards Northwest, which are bounded by JFZ and GFZ. In general, the lowest channel gradient occurs along the subsidence zone. Furthermore, the channel gradient experiences a noticeable drop along the CMF, which is associated with river avulsion and migration and is prone to aggradation (Figs. 12A, 12B, 12C, 13 and 14). Downward the GFZ towards the outlet of the Cinzas River, we observe a high channel gradient and base-level fall along the third tectonic zone (Figs. 8, 10A and 11).

Both the swath profiles SP 2 and SP 3 highlight the topographic responses along the distinctive tectonic zones and disclose three marked blocks, as well as the topographic differences among them and between the sectors of the Cinzas and Laranjinha rivers. Major faults play a significant role in the topography, and the compartments are bounded by JFZ and

GFZ. However, the Figueira Fault (FF) also plays an essential role for the southeasternmost edge of the subsidence zone, presenting a sharp change of the local relief, similarly in GFZ.

It is relevant to emphasize that the elevation differences between the uplift and subsidence zones are more pronounced along the reach of the Laranjinha river than the Cinzas' when compared to swath profiles SP 2 and SP 3. Furthermore, the subsidence zone is flatter in the sector of the Laranjinha river than the Cinzas'. The north-eastern edge of the subsidence zone is bounded by JSAFZ, which is associated with a sharp southwest-facing step (SP 4, Fig. 11). The Laranjinha Graben System is also clearly expressed in the topographic profiles SP 3 and 4 and it is placed between FF and GFZ along the NNW-trending and between SJCFZ and a horst along the NE-trending (Fig. 11). Comparing the profiles SP 3 and 4, the elevation difference is more pronounced towards the southwest, associated with the fault scarp along the SJCFZ (ca. 450 m).



SJCFZ: São Jerônimo-Curiúva; SSF: São Sebastião; JFZ: Jacutinga; GFZ: Guaxupé; JSAFZ: Jacarezinho-Santo Anatócio; CMF: Conselheiro Mairinck; FF: Figueira; SAPF: Santo Antônio da Platina.

**Figure 11.** Topographic swath profiles across the Cinzas Catchment. Swath widths are 20 km for SP 2 and 10 km for the others. S1 and S2 indicate surfaces characterized by isolated peaks ac. 1,000 m and 800-850 m. The inset present the position of the swath profiles in the Cinzas catchemnt.

Downward the JFZ to reach the GFZ, avulsion and migration mechanisms occurred, e.g., crevasse splay, and large flood-plains were produced in association with gentler gradients in both the Cinzas and Laranjinha rivers along the subsidence zone (Figs. 10B and 12C). Therefore, paleochannels and terraces from the Late Pleistocene (from ~ 106 ka to 20 ka) are common in this sector, related to the highest sinuosity reaches (Figs. 12A, 12C and 13).

Reaches of the Laranjinha River and other major tributaries are currently incised into landslide deposits (debris flows and mudflows) (Fig. 12D) from the Late Pleistocene (87982 ± 5249 BP, for mudflows), which resulted from active fault escarpments controlled by NW-SE/NNW-SSE- and ENE-WSW/NE-SW-trends along GFZ (Figs. 9B, 13 and 14) as well as SJCFZ. We observe local preservation of the source of a landslide along the GFZ escarpment (Fig. 14). In contrast,

towards the upper/middle course of the Cinzas catchment (uplift zone) a high incision of channels prevails, flowing directly over the Paleozoic bedrock or Mesozoic basaltic dykes associated with knickpoints along the faults (Fig. 12F, 12G and 12H).

## DISCUSSION

### Bedrock inheritance as an influencing factor on the geomorphic channel responses

Distinguishing between a tectonic and non-tectonic signal has been proved difficult (Kirby and Whipple 2012). At the scale of larger catchments, much of the variability in channel gradients, and therefore river incisions, can be explained by tectonics, climate change, base-level variations, or contrasting



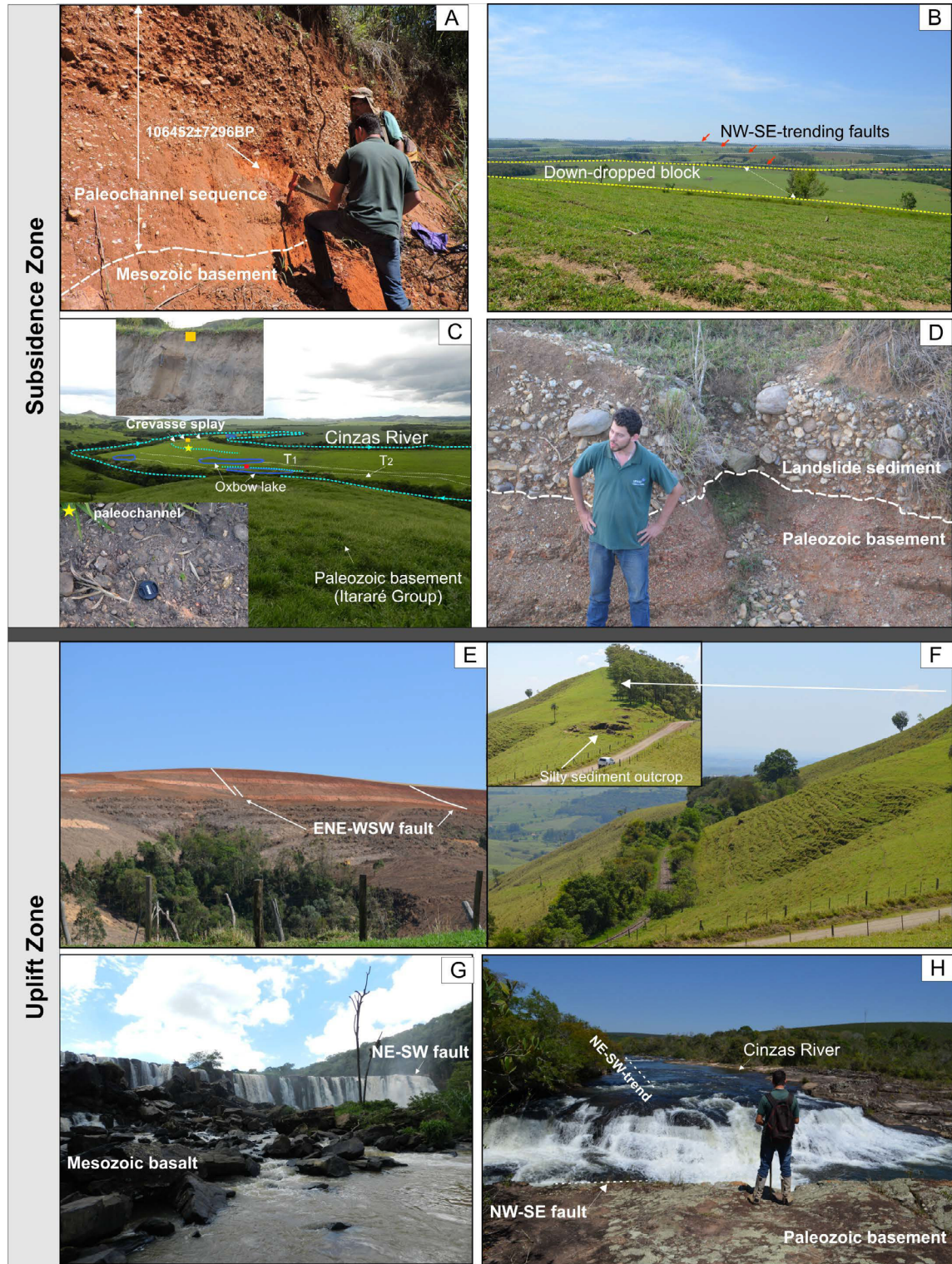


**Figure 12.** Contrasting geomorphic responses between distinctive tectonic zones of the Cinzas Catchment. (A) Paleochannel sequence of the Cinzas River; (B) NW-trending graben associated with SJCFZ rejuvenation along the Laranjinha Graben System; (C) Avulsion and migration of the Cinzas River;  $T_1$  ( $41573 \pm 5436$  BP) and paleochannel separating  $T_1$  and  $T_2$  ( $20707 \pm 1771$  BP); (D) Landslide associated with the SJCFZ; (E) São Sebastião Fault is affecting the Paleozoic; (F) Highlands on silty sediments and prevailing mass movement processes; (G) Knickpoint along a tributary of the Cinzas River associated with the JFZ; (H) Knickpoint along Cinzas River associated with the TF. The location of the photos is provided in Figure 10B.

lithology (e.g., Wobus *et al.* 2006, Whittaker *et al.* 2007, Burbank and Anderson 2012, Ferrier *et al.* 2013). Furthermore, regions with heterogeneous bedrock make the goal of understanding the interactions between different factors and recognizing the prevailing forcing(s) harder (cf. Marques *et al.* 2021, Peifer *et al.* 2021).

Our results demonstrate that the geomorphic responses of the analysed rivers are cannot be justified by a uniquely lithological influence, whether contrasting lithology or lithological boundaries presented. The major faults in the study area have shown recurrent activity over time and a substantial effect on the evolution of the Paraná Basin as pointed out by the

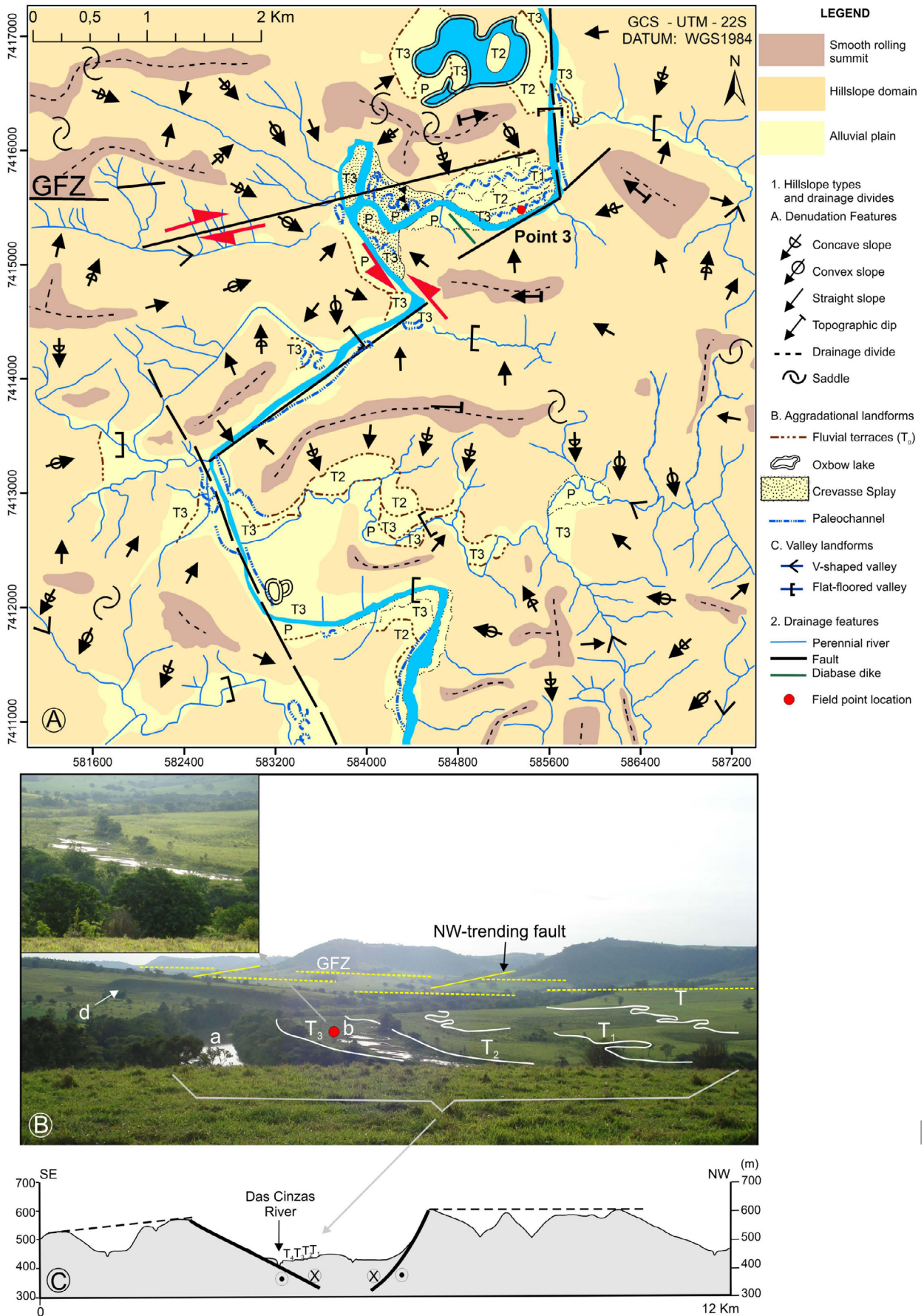


**Figure 13.** Cinzas river avulsion and incision in response to lateral tilting towards southwest. (A) Detailed geomorphological map of the key area; (B) Fluvial terraces and paleochannel: a – current channel of the Cinzas river; b – paleochannel reach; d – diabase dyke; T to T<sub>3</sub> constitute the successive terraces formed by avulsion and incision; P – current alluvial plain; (C) Red arrows indicate the sense of the slip fault. Topographic profile of the key area; location of the map and photos is provided in Figure 10B.

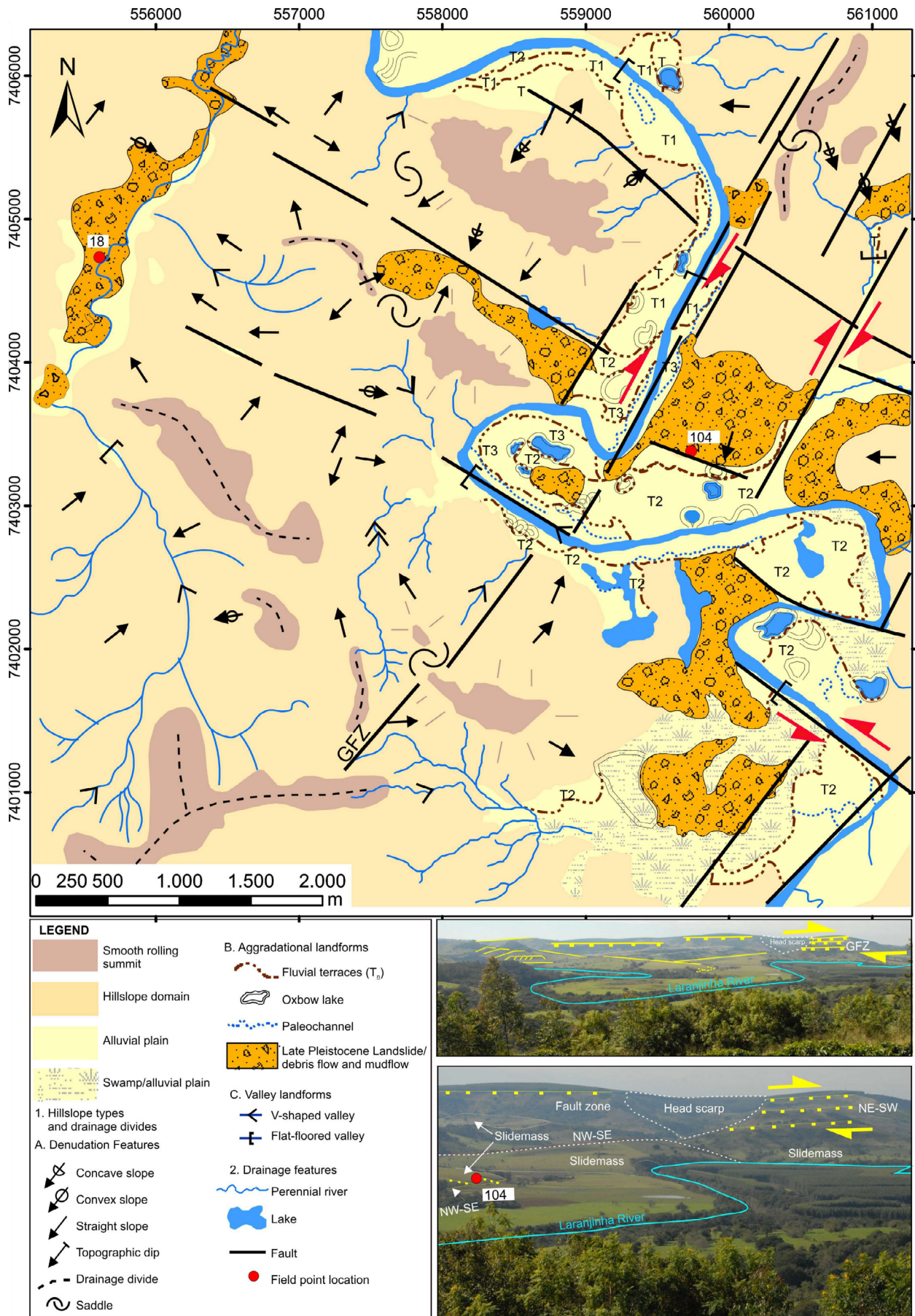


**Figure 14.** Aggradation and avulsion in response to NW-SE and NW-SE-trending normal faults along the GFZ in the Larajinha catchment. The head scarp marks the source of part of the landslides along the GFZ; point 18 in the map sets the mudflow occurrence from the Late Pleistocene ( $87982 \pm 5249$  BP); red and yellow arrows indicate the sense of the slip fault; location of the map and photos is provided in Figure 10B.

literature. These structures coincide with lithological boundaries, which may obscure the tectonic influence on the post-rifting landscape evolution. Despite the geomorphic responses suggesting a limited effect of lithological/boundary contrasting on the major channels, they demonstrate that the bedrock inheritance plays a meaningful role through the pre-existing fault zones. For instance, despite the channel steepening along the JFZ, the lithology remains the same throughout the fault zone and surrounding areas (Figs. 8 and 9). We thus discuss the influence of these bedrock features and other factors on geomorphic responses as follows.

In the Cinzas catchment, we observe an interplay between knickpoints, a high  $SL_{relative}$  index corresponding to a high channel gradient, and the major faults.

A knickpoint is a straight geomorphic response resulting from tectonic perturbations, climate changes, lithological control, or a slip on a fault (Menier *et al.* 2017). Moreover, knickpoints divide an incised downstream portion of the catchment that has adjusted to perturbation, usually called as transient landscape, from the upstream catchment that is still to respond, often referred to as reliquial or relict landscape (Crosby and Whipple 2006, Whittaker *et al.* 2007, Marques *et al.* 2021). The resulting migration of the knickpoint creates a wave of incision which progressively spreads the signal of boundary condition change throughout the catchment (Tucker and Whipple 2002, Whittaker *et al.* 2010, Whittaker 2012).

Therefore, assessing knickpoints and the stream-gradient index along the longitudinal profile is a valuable key for understanding the significant processes in the landscape. Furthermore, as the knickpoints spread outward the forcing, they induce incision erosion, resulting in steeper hillslopes and a tendency to creep and cause landslides (c.f. Marques *et al.* 2021). In contrast, aggradation waves also spread outward the disturbance source (Burbank and Anderson 2012). Therefore, as the knickpoints radiate the change upwards throughout the catchment, corresponding terraces may be created. If dating is possible, the terraces may provide the age of the perturbation and the knickpoints migration rate, as well as the incision rate (Crosby and Whipple 2006).

Our findings show an association between some knickpoints and basal dykes, as well as lithological boundaries, e.g., along the SJCFZ in the upper source of the Cinzas River and along the Paleozoic-Mesozoic boundary respectively (Fig. 8). For the latter case, the resistant units (i.e., Botucatu and Serra Geral Formations) along the GFZ and their lithological/boundary contrasting with the more erodible Palaeozoic silty/clayey sediments (i.e., Rio do Rasto Formation) likely present an influence on local relief and incision along the escarpment and the boundary between the distinctive zones. However, the positions of most of the knickpoints do not correlate with any lithological boundaries or contrasting lithology, nor are they located at a single threshold drainage area (Figs. 8 and 9). In contrast, most of the knickpoints fit with the high  $SL_{relative}$  values (high channel gradient) and the bedrock fault zones. Furthermore, most of the steeper channel reaches (high  $SL$  index values) are not associated with resistant and less fractured rocks.  $SL$  index variations occur in the

same lithology (e.g., Itararé Group, Rio do Rasto and Serra Geral formations), which provides a compelling argument for the tectonic factor (cf. Wobus *et al.* 2006, Whittaker *et al.* 2007, Kirby and Whipple 2012).

The sharp changes of the channel gradient responses of both the Laranjinha and Cinzas Rivers along the SJCFZ near their sources also call for attention, since they are non-coherent considering the higher lithological strength of the Furnas Formation concerning the Itararé Group. The knickpoints with elevations from 490 m to 580 m associated with the JFZ suggest an intermediate and transient landscape seeking adjustments to boundary conditions by the knickpoints migration along a wide knickzone (Figs. 8 and 9).

We also observe a clear relation between the pre-existing fault sectors (e.g., GFZ, JFZ and SJCFZ) and a high symmetry factor (Fig. 6), channel sinuosity changes evidenced mainly by a sinuosity drop while crossing the NE-SW-trending FF and JFZ (Fig. 7), a channel gradient increase and knickpoints (Figs. 8, 9 and 10A), suggesting a straight interaction with the bedrock inheritance. Therefore, the evidences allow us to point out that the bedrock inheritance played a relevant role in the geomorphic channel responses and hence the landscape evolution during the Cenozoic more due to major fault zones and lineaments than lithological/boundary contrasting.

### River's signature to tectonic rejuvenation

As already mentioned, the geomorphic responses show a straight association with the bedrock fault zones (Figs. 8 and 9). Additionally, the association between the two Late Pleistocene landslide clusters and the GFZ and SJCFZ (Fig. 10B) along the Laranjinha Graben System, as well as their small, shallow and fault-driven geometry (Fig. 14) and the existing strike-slip faults, enables us to think of them as a result of seismic activity and not of climate-driven erosion (cf. Guo *et al.* 2020). This direct relation between fault-driven landslide primarily along the Pre-Cenozoic fault zones and the noted geomorphic responses (e.g., channel pattern instability, T anomalous values, avulsion and migration, incision increase, high basin asymmetry) indicates that a fault rejuvenation likely triggered a transient landscape response via landsliding during the Late Pleistocene, as well as a knickpoint retreat and associated fluvial incision.

Knickpoint distribution in the Cinzas catchment and the channel gradient signatures indicate that the channels are responding to pulses of incision, likely initiated through regional base-level fall which have affected the Cinzas trunk river and spread towards its major tributary (cf. Crosby and Whipple 2006, Whipple and Tucker 1999). In fact, channel profiles of both the Cinzas and Laranjinha Rivers exhibit a downstream increase in channel gradient, which is consistent with a transient profile adjustment to an increase in rock uplift rate/base level fall (cf. Kirby and Whipple 2001, Crosby and Whipple 2006, Whittaker *et al.* 2007). Instead, knickpoint distribution along distinct elevations, including near the trunk river around its outlet suggests more than one pulse of rock uplift/base-level fall in the Cinzas catchment (cf. Wobus *et al.* 2006). For example, the knickpoints along SJCFZ are aligned

and laid on different elevations (Figs. 8 and 9), which likely suggests a boundary between zones with different uplift rates (cf., Wobus *et al.* 2006, Burbank and Anderson 2012), indicating a tectonic influence for these geomorphic responses.

These results enhance the interpretation of different rock uplift rates throughout the Cinzas catchment and stress concentration resulting in fault rejuvenation (cf. Wobus *et al.* 2006). Therefore, our observations reveal transient responses in a nonequilibrium landscape, associated with coupled tectonic rejuvenation and bedrock inheritance.

The joint analysis of geomorphic responses as well as both the geophysical data and faulting-driven landslides, in addition to topography assessment, show three tectonically distinguished zones (Fig. 11). The first zone, in the upper Cinzas catchment, constitutes an upland with peaks over 1,000 m in altitude and levelled with a surface S1 aged at ac. 22 Ma (Franco-Magalhães *et al.* 2010). On the other hand, a relict geomorphic surface in different regions corresponding with S1 lies on ca. 800 m aged at ac. 35 Ma (cf. Riffel *et al.* 2015). Therefore, the higher elevation and younger age of the S1 make the interpretation of a tectonic surface and not a classical relict geomorphic surface favourable.

Our results thus suggest that the S1 surface is raised about two hundred meters in this uplift zone of the Cinzas catchment compared to other regions in a similar setting. In addition, we find high local relief along the fault zones in this upland portion. Also noteworthy is that even soft lithologies outcrop and sustain the highlands of this uplift zone, usually presenting associated mass movement processes. In contrast, soils and even shallow saprolites are unusual. These results are consistent with the transpressional regime indicated by this sector's fault kinematics and paleostress analysis (Fig. 5). Furthermore, we were unable to find ferruginous duricrusts or even deep saprolite in the upper and middle Cinzas catchment, suggesting the hypothesis that a tectonic forcing prevented an intense weathering, or the most likely scenario, that deep saprolites and scattered ferruginous duricrusts have been deeply eroded from the Neogene to the Quaternary. Therefore, our results are congruent with the exhumation history associated with the tectonic rejuvenation of the SJCFZ from the Miocene onwards (cf. Franco-Magalhães *et al.* 2010).

Moreover, considering the exhumation history of the PGA (e.g., Cobbold *et al.* 2001, Franco-Magalhães *et al.* 2010, Cogné *et al.* 2011) and the tectonic rejuvenation due to far-field stress (e.g., Cobbold *et al.* 2001, Riccomini *et al.* 2004, Cogné *et al.* 2011), this uplift zone is likely a result of an expressive regional uplift due to the recurring post-rifting transpressional regimes coupled with denudational isostatic rebound and the reactivation of weakness zones (cf. Silva and Sacek 2019). Such a rejuvenation process was responsible for changing the source area and the transport trending of sedimentary supply in the offshore Santos Basin, indicating this portion of the PGA as a meaningful supply source to the offshore basins (e.g., Franco-Magalhães *et al.* 2010).

The second tectonic zone characterizes the lowlands of the middle course of the Cinzas catchment with an average elevation of ac. 500 m. and low local relief. It also tends to a flat

landscape associated with prevailing aggradation and channel avulsion/migration, as well as NW-trending grabens development with straight relation with low gravimetric and magnetic anomalies (Figs. 3 and 10B) and strike-slip faults. Thus, these interactions support that a tectonic influence (subsidence/lower uplift rate) plays a meaningful role for this zone, most likely from the Late Pleistocene to Early Holocene as detailed further on.

The third tectonic zone ranges from the GFZ to the Cinzas catchment outlet, displaying high local relief along the GFZ and an average elevation of ac. 600 m which is tilted Northwest and marked by a base-level fall combined with high channel gradient (Figs. 8, 9 and 11). In addition, this zone shows remnants of peaks with elevations ac. 850 m (see SP1 and SP3 in Fig. 11) and ac. 750 m (SP2; Fig. 11) along the GFZ. The interactions between seismicity, geophysical data and geomorphic responses enhance a tectonic influence for this sector and provide the hypothesis of an association with possible stress concentration (cf. Mooney *et al.* 2012) along the GFZ and the critical weakness zone represented by the boundary of the Paranapanema Craton (Fig. 1).

### Fault rejuvenation in a post-rifting setting: considerations about prime targets

Geophysical studies carried out in the PGA region point out to an association between Mesozoic crustal thinning, due to a mantle plume referred to as the Trindade Plume and related Atlantic opening process. The dyke swarms added to the tectonic rejuvenation along NW/NE-trending lineaments and major pre-existing faults (Ferreira 1982, Strugale *et al.* 2007, Fernandes 2010).

Crustal thinning areas are a prime target to seismic activity in the Brazilian territory (Assumpção 1998, Assumpção *et al.* 2016). Furthermore, the coincidence of the southern boundary of the Paranapanema Craton with the lower course of the Cinzas catchment (Fig. 1) allows us to consider this portion as a substantial stress concentrator (e.g., Mooney *et al.* 2012, Talwani 2014, 2017). The NE-SW trend coincides with the southern edge of the Paranapanema Craton (Fig. 1A) which represents a contrasting crustal thickness zone (e.g., Mantovani *et al.* 2005), suggesting an interaction between this direction and the Upper Proterozoic bedrock structures, which controlled the development of the Paraná Basin. Therefore, these joined weakness features and structures suggest that the Cinzas catchment area embraces a complex mosaic of tectonic elements favourable to post-rift tectonic rejuvenation, as also observed in other large catchments in old rift regions in Brazil, such as the Quebra-Anzol catchment in the Alto Paranaíba Arch (cf. Marques *et al.* 2021).

Our results show that part of the SJCFZ coincides with the aligned boundary between high and low Bouguer gravity anomalies along the middle/lower course of both the Cinzas and Tibagi catchments, and it appears to control two elongated low Bouguer anomalies (Fig. 3B). Furthermore, the coinciding of this low gravity anomaly in the Cinzas catchment and the intersection between the GFZ and SJCFZ (Fig. 3) calls

for attention, also matching the NW-SE-trending Laranjinha Graben system from the Late Pleistocene (Figs. 3, 4 and 10B). Moreover, in the Tibagi catchment the low gravity anomaly portion coincides with a seismoactive sector of low/moderate magnitude earthquakes (Figs. 3A and 3B).

These results suggest a link between the existing seismic/geophysical data, the Late Pleistocene faulting-driven landslides along intersection zones between the pre-existing fault zones SJCFZ and GFZ, and the NW-trending Laranjinha graben system (Figs. 10B and 14). We also observe that the geometric arrangement shown in the SP4 (Fig. 11) suggests that the SJCFZ is a detachment faulting and the Laranjinha Graben System is associated with developing a trailing-edge basin's hanging wall (cf. Swaney *et al.* 2010). Our results enable the hypothesis that the two highlighted sectors of low gravimetric anomalies may be related to the rejuvenation of shallow NW-trending rifting structures bounded by NE-trending faults. Hence, it is reasonable to consider that a Quaternary tectonic rejuvenation has taken place in this portion of the PGA, preferably by recurrent tectonic activation along the intersection of the major NE-SW and NW-SE faults, GFZ and SJCFZ respectively.

It calls attention to this Late Pleistocene tectonic activity which does not appear to be an isolated event, as studies on distinctive subjects point out to tectonic reactivation along major lineaments in the Paraná Basin area and surroundings during the Late Pleistocene (e.g., Riccomini *et al.* 1989, Strugale *et al.* 2007, Peyerl *et al.* 2018, Reis *et al.* 2020).

The kinematic and paleostress analysis of the major fault zone domains of the Cinzas catchment demonstrate variation on the stress regime (Fig. 5) as evidenced in previous studies in the PGA setting (e.g., Riccomini *et al.* 1989, Riccomini and Assumpção 1999, Riccomini *et al.* 2004, Salamuni *et al.* 2017, Peyerl *et al.* 2018, Santos J.M. 2019). Despite the limited kinematic data, our results suggest that this variation occurs

either internally or between the domains, likely indicating an episodic fault behaviour on both the temporal and spatial scale, as expected in low tectonic strain settings (Crone *et al.* 2003, Liu *et al.* 2011).

We identify four stress regimes, three strike-slip and one extensional, which we interpret, based on the paleostress analysis, sediments dating and fieldwork (intersecting relations between the different fault groups and geomorphic features), as corresponding to deformation events of post-rift rejuvenation ( $D^1$  to  $D^4$ ) as described by previous studies (e.g., Riccomini *et al.* 1989, Salamuni *et al.* 2003, Riccomini *et al.* 2004). Furthermore, the fault kinematic analysis shows that these events reactivated the major fault zones through the prevalence of strike-slip and minor normal movement (Fig. 5).

Table 2 summarizes the results of the fault kinematics and paleostress analysis in the Cinzas catchment and a proposal of correlation with previous studies.

The earliest record of post-rifting rejuvenation we can find ( $D^1$ ) corresponds to the Neogene (Miocene) strike-slip event, which is present in both NE and NW major fault zones (GFZ and JSAFZ). Thermochronological data reports this as one of the most important post-rifting tectonic rejuvenation events, with stress concentration mainly along the SJCFZ and hence high cooling and denudation rate in this PGA region, (Franco-Magalhães *et al.* 2010, Cogné *et al.* 2012). Despite not identifying kinematic indicators associated with this Miocene event along the SJCFZ, our results show that it is reasonable to consider that the uplift zone in the upper course of the Cinzas catchment, as well as the aligned knickpoints along the SJCFZ and the base-fall indicators, may be related to such a tectonic event.

In addition to the Miocene rejuvenation, three Quaternary events are registered. The earlier ( $D^2$ ), from Late Pleistocene-Holocene, played a meaningful role in the landscape of the Cinzas

**Table 2.** Paleostress fields with the sectors of the major fault zones in the Cinzas Catchment.

Sector	SHmax	SHmin	Stress Regime	Active Structures	Age*
SJCFZ	~E-W <sup>D4</sup> (ENE)	NNW-SSE	Strike-slip transpressional regime	NW-SE master faults and Y and R conjugate faults around the ENE-WSW trend	Current
	~E-W <sup>D4</sup> (WNW)	NNE-SSW		NW-SE left-lateral strike-slip faults and ~E-W right-lateral strike-slip faults; secondary oblique strike-slip faults	
JFZ	Extensional NW-SE <sup>D3</sup> (N331/05)	Subvertical (N230/65)	Extensional	ENE-WSW normal faults	Early Holocene
Central	NW-SE <sup>D2</sup>	NE-SW	Strike-slip transtensional stress regime;	Conjugate strike-slip faults with ~N-S and NE-SW trends ~WNW to NW right-lateral strike-slip faults	Late Pleistocene-Holocene
GFZ	NE-SW <sup>D1</sup>	NW-SE	Strike-slip transtensional stress regime	NW-SE and ~E-W left-lateral strike-slip faults	Neogene (Miocene)
JSAFZ			Strike-slip transpressional stress regime	Conjugate NNE-SSW right-lateral strike-slip and WNW-ESE left-lateral strike-slip faults	

\*Inferred age from Riccomini *et al.* (1989, 2004).

catchment, which triggered a graben system along intersection sectors between the GFZ/FF and SJCFZ. This transtensional paleostress regime influenced the channel pattern of the trunk river and its major tributary, resulting in landslides clusters as well as avulsion and migration of the major rivers. A post-Pliocene denudation intensification appears to be combined with such a rejuvenation (cf. Riffel *et al.* 2015).

We also identified an extensional event ( $D^3$ ) along the JFZ domain. We interpreted it as corresponding to the Early Holocene extensional regime reported by previous studies (c.f. Riccomini and Assumpção 1999, Riccomini *et al.* 2004). Later, this paleostress regime changed to the current transpressional regime ( $D^4$ ) with  $\sim$ E-W horizontal compressive  $SH_{max}$ , which affected both NE and NW major faults in the Cinzas catchment, the JFZ and SJCFZ respectively. Furthermore, the most recent pulse of knickpoints, which are positioned near the trunk river in the surrounding area of the outlet, coupled with base-level fall marked by gradient increase of both the Cinzas and Laranjinha Rivers, suggest a probable relationship to this current stress field.

Therefore, our results show that, during the Neogene, the major NE faults (linked to roots of Proterozoic shear zones) were reactivated due to a transtensional stress regime, whereas the prominent NW faults rejuvenated according to a transpressional stress regime, both under a NE-SW  $SH_{max}$  associated with a strike-slip stress field ( $D^1$ ). In the Late Pleistocene, the  $SH_{max}$  rotated towards NW-SE ( $D^2$ ) and the transtensional stress gathered strength along the intersection zones between the NE and NW major faults, triggering a graben system with NE and NW boundaries. Landslide clusters added to a remarkable migration and avulsion of the major rivers are also present. This strike-slip paleostress-field changes to an effective extensional regime with the persistence of the NW-SE  $SH_{max}$  ( $D^3$ ) during the Early Holocene, later giving rise to a current transpressional stress regime ( $D^4$ ) along both the NE and NW major faults.

The link between the paleostress data and the geomorphic river responses, coupled with the bedrock inheritance influence, provides compelling evidence of recurring tectonic rejuvenation in the study area. Despite several models attempting to explain the usual Neogene tectonic rejuvenation in ancient rifting settings, a definitive solution remains uncertain. Based on our results, it is reasonable to consider that the range of stress concentrators consisted of various weakness zones of different natures, such as the expressive pre-existing fault zones, boundaries of cratons and differential lithospheric rheology and strength, presents perturbations triggered by more than one driver. Hence, it is more likely that a combined mosaic of superimposed mechanisms, such as the far-field stress coupled with denudational isostatic rebound and the influence of pre-existing crustal weakness, explains the tectonic rejuvenation of the PGA region, which previous studies have invoked (cf. Silva and Sacek 2019, Silva 2021).

## CONCLUSIONS

In this work, we explore geomorphic responses of rivers and their interactions with tectonic rejuvenation and bedrock

inheritance. A compelling relationship between the pre-existing fault zones and high basin symmetry factor, channel sinuosity change, channel gradient increase and knickpoints evidences a straight interaction with the bedrock inheritance. Thus, we show that the bedrock inheritance, played a relevant role in the geomorphic channel responses (hence, the landscape evolution) less due to lithological/boundary contrasting and more due to major fault zones and lineaments. We also demonstrate that the interactions between anomalous river signatures and the major bedrock fault zones in the study area are responses to post-rifting tectonic rejuvenation coupled with bedrock inheritance. The results reveal geomorphic and geological signals associated with an unsteady landscape mainly due to strike-slip tectonic events, from the Neogene onwards, preferentially through stress concentrators such as intersecting sectors of pre-existing fault zones and surrounding areas of craton boundaries. Our study demonstrates that the NW and NE-trending fault zones, SJCFZ and GFZ, respectively, acted as coupled structures and a prime target for post-rift tectonic rejuvenation. The kinematic and paleostress analysis of the major fault zone domains present variation on the stress regime as evidenced in previous studies in the PGA setting. In addition to the current strike-slip stress regime, we identify three paleostress regimes, two strike-slip and one extensional, consistent with the post-rift tectonic rejuvenation events previously pointed out for the PGA region.

As described in previous studies, the range of stress concentrators in the study area consisted of various weakness zones of different natures. For instance, the expressive pre-existing fault zones, boundaries of cratons, and differential lithospheric rheology and strength, may join perturbations triggered by a mosaic of driving mechanisms. Hence, it is more likely that a combined mosaic of superimposed mechanisms has been invoked by previous studies, such as the far-field stress coupled with denudational isostatic rebound and the influence of pre-existing crustal weakness, explains the tectonic rejuvenation of the PGA region. However, further studies on fluvial erosion rates and internal forcing, such as lithological strength influence and drainage reorganization, are required to provide more clues for better distinguishing the role of the diverse driven mechanisms in the study area and surroundings.

## ACKNOWLEDGEMENTS

We thank the Fundação de Amparo à Pesquisa do Estado de São Paulo – FAPESP (2014/09202-8) for financial support to the research project “Morphogenesis of the das Cinzas catchment (PR): landforms, sedimentation and neotectonics study”. The second, third, fourth and fifth authors also thank CNPq for the PQ grants (307951/2018-9), (310734/2020-7), (302677/2016-0) and (307738/2019-1), respectively. The scientific results were obtained using Win-Tensor, a software developed by Dr. Damien Delvaux, Royal Museum for Central Africa, Tervuren, Belgium. Finally, we would like to thank Dr Claudio Riccomini and two anonymous reviewers for their thoughtful comments and suggestions on our manuscript.

## ARTICLE INFORMATION

Manuscript ID: 20210002. Received on: 01 JUN 2021. Approved on: 07 FEB 2022.

How to cite: Santos M., Ladeira F.S.B., Batezelli A., Nunes J.O.R., Salamuni E., Silva C.L., Molina E.C., Moraes I.C. Interactions between tectonics, bedrock inheritance and geomorphic responses of rivers in a post-rifting upland (Ponta Grossa Arch region, Brazil). *Brazilian Journal of Geology*, 52(1):e20210002, 2022. <https://doi.org/10.1590/2317-4889202220210002>

M.S. conceived the project and planned the experiments, carried out the literature review, the field work, sampling, the data processing, the data analysis and interpretation, wrote the manuscript, and edited the figures; F.L. collaborated with the project and field works, sampling and reviewed the manuscript; A.B. collaborated with the project, field works, sampling, the sedimentary and stratigraphic analysis and improved the manuscript through corrections and suggestions; J.N. collaborated with the project and field works, sampling and the detailed geomorphological map; E.S. collaborated with the field works, carried out the structural and paleostress analysis and made the first draft of this item, and improved the manuscript through corrections and suggestions; C.S. collaborated with the geomorphic analysis and improved the manuscript through corrections and suggestions; E.M. carried out the geophysical maps and improved the manuscript through corrections and suggestions; I.M. collaborated with the data processing and the Figure 10.

Competing interests: The authors declare no competing interests.

## REFERENCES

- Artur P.C., Soares P.C. 2002. Paleoestruturas e petróleo na Bacia do Paraná, Brasil. *Revista Brasileira de Geociências*, **32**(4):433-448.
- Assumpção M. 1998. Seismicity and stresses in the Brazilian passive margin. *Bulletin of the Seismological Society of America*, **88**(1):160-169. <https://doi.org/10.1785/BSSA0880010160>
- Assumpção M., Dias F.L., Zevallos I., Naliboff J.B. 2016. Intraplate stress field in South America from earthquake focal mechanisms. *Journal of South American Earth Sciences*, **71**:278-295. <https://doi.org/10.1016/j.jsames.2016.07.005>
- Assumpção M., Ferreira J., Barros L., Bezerra H., França G.S., Barbosa J.R., Menezes E., Ribotta L.C., Pirchiner M., Nascimento A., Dourado J.C. 2014. Intraplate seismicity in Brazil. In: Talwani P. (Ed.). *Intraplate earthquakes*. Cambridge: U. P., p. 50-71.
- Baldwin J.A., Whipple K.X., Tucker G.E. 2003. Implications of the shear stress river incision model for the timescale of post-orogenic decay of topography. *Journal of Geophysical Research*, **108**(B3). <https://doi.org/10.1029/2001JB000550>
- Beeson H.W., McCoy S.W. 2020. Geomorphic signatures of the transient fluvial response to tilting. *Earth Surface Dynamics*, **8**:123-159. <https://doi.org/10.5194/esurf-8-123-2020>
- Bianchi M.B., Assumpção M., Rocha M.P., Carvalho J.M., Azevedo P.A., Fontes S.L., Dias F.L., Ferreira J.M., Nascimento A.F., Ferreira M.V., Costa L.S.L. 2018. The Brazilian Seismographic Network (RSBR): improving seismic monitoring in Brazil. *Seismological Research Letters*, **89**(2A):452-457. <https://doi.org/10.1785/0220170227>
- Bishop P. 2007. Long-term landscape evolution: linking tectonics and surface processes. *Earth Surface Processes and Landforms*, **32**(3):329-365. <https://doi.org/10.1002/esp.1493>
- Bishop P., Goldrick G. 2010. Lithology and the evolution of bedrock rivers in post-orogenic settings: constraints from the high-elevation passive continental margin of SE Australia. *Geological Society Special Publication*, **346**:267-287. <https://doi.org/10.1144/SP346.14>
- Bizzi L.A., Schobbenhaus C., Vidotti R.M., Gonçalves J.H. (Eds.). 2003. *Geologia, tectônica e recursos minerais do Brasil*: texto, mapas e SIG. Brasília: CPRM, 642 p.
- Burbank D.W., Anderson R.S. (Eds.). 2012. *Tectonic geomorphology*. Oxford: Wiley-Blackwell, 454 p.
- Câmara G., Souza R.C.M., Freitas U.M., Garrido J. 1996. Spring: Integrating remote sensing and GIS by object-oriented data modelling. *Computers & Graphics*, **20**(3):395-403. [https://doi.org/10.1016/0097-8493\(96\)00008-8](https://doi.org/10.1016/0097-8493(96)00008-8)
- Cobbold P.R., Meisling K.E., Mount V.S. 2001. Reactivation of an obliquely rifted margin, Campos and Santos Basins, Southeastern Brazil. *AAPG Bulletin*, **85**(11):1925-1944. <https://doi.org/10.1306/8626D0B3-173B-11D7-8645000102C1865D>
- Cogné N., Cobbold P.R., Riccomini C., Gallagher K. 2013. Tectonic setting of the Taubaté Basin (Southeastern Brazil): Insights from regional seismic profiles and outcrop data. *Journal of South American Earth Sciences*, **42**:194-204. <https://doi.org/10.1016/j.jsames.2012.09.011>
- Cogné N., Gallagher K., Cobbold P.R. 2011. Post-rift reactivation of the onshore margin of southeast Brazil: evidence from apatite (U-Th)/He and fission-track data. *Earth and Planetary Science Letters*, **309**(1-2):118-130. <https://doi.org/10.1016/j.epsl.2011.06.025>
- Cogné N., Gallagher K., Cobbold P.R., Riccomini C., Gautheron C. 2012. Post-breakup tectonics in southeast Brazil from thermochronological data and combined inverse-forward thermal history modeling. *Journal of Geophysical Research*, **117**(B11). <https://doi.org/10.1029/2012JB009340>
- Cordani U.G., Ramos V.A., Fraga L.M., Cegarra M., Delgado I., Souza K.G., Gomes F.E.M., Schobbenhaus C. 2016. Tectonic map of South America=Mapa tectônico de América del Sur=Mapa tectônico da América do Sul. Available at: <http://rigeo.cprm.gov.br/xmlui/handle/doc/16750>. Accessed on: June 20, 2021.
- Crone A.J., De Martini P.M., Machette M.N., Okumura K., Prescott J.R. 2003. Palaeoseismicity of two historically quiescent faults in Australia — implications for fault behaviour in stable continental regions. *Bulletin of the Seismological Society of America*, **93**(5):1913-1934. <https://doi.org/10.1785/0120000094>
- Crosby B.T., Whipple K.X. 2006. Knickpoint initiation and distribution within fluvial networks: waterfalls in the Waipaoa River, North Island, New Zealand. *Geomorphology*, **82**(1-2):16-38. <https://doi.org/10.1016/j.geomorph.2005.08.023>
- Delvaux D., Sperner B. 2003. Stress tensor inversion from fault kinematic indicator and focal mechanism data: The TENSOR program. In: Nieuwland D. (Ed.). *New insights into structural interpretation and modelling*. London: Geological Society, Special Publications, **212**:75-100.
- Engelmann de Oliveira C.H., Jelinek A.R., Chemale Jr. F., Cupertino J.A. 2016. Thermotectonic history of the southeastern Brazilian margin: evidence from apatite fission track data of the offshore Santos Basin and continental basement. *Tectonophysics*, **685**:21-34. <https://doi.org/10.1016/j.tecto.2016.07.012>
- ESRI. 2011. *ArcGIS Desktop*: Release 10. Redlands: Environmental Systems Research Institute.
- Fernandes M.A. 2010. *Análise, modelagem e interpretação de dados gravimétricos no lineamento Guapiara – região sudeste do estado de São Paulo*. MS Dissertation, IGCE, Universidade Estadual Paulista “Júlio de Mesquita Filho”, Rio Claro, 84 p.
- Ferreira F.J.F. 1982. *Geologia da Bacia do Paraná*: alinhamentos estruturais-magnéticos da região centro-oriental da Bacia do Paraná e seu significado tectônico. IPT, Relatório Técnico, 143-166.
- Ferreira F.J.F., Moraes R.A.V., Ferrari M.P., Vianna R.B. 1981. Contribuição ao estudo do Alinhamento Estrutural de Guapiara. In: Simpósio Regional de Geologia, 1981. *Anais...* Curitiba, v. 3, p. 226-240.
- Ferrier K.L., Huppert K.L., Perron T. 2013. Climatic control of bedrock river incision. *Nature*, **496**:206-211. <https://doi.org/10.1038/nature11982>
- Franco-Magalhães A.O.B., Cuglieri M.A.A., Hackspacher P.C., Saad A.R. 2014. Long term landscape evolution and post-rift reactivation in the southeastern Brazilian passive continental margin: Taubaté Basin. *International Journal of Earth Sciences*, **103**:441-453. <https://doi.org/10.1007/s00531-013-0967-4>



- Franco-Magalhães A.O.B., Hackspacher P.C., Glasmacher U.A., Saad A.R. 2010. Rift to post-rift evolution of a "passive" continental margin: the Ponta Grossa Arch, SE Brazil. *International Journal of Earth Sciences*, **99**(7):1599-1613. <https://doi.org/10.1007/s00531-010-0556-8>
- Gailleton B., Sinclair H.D., Mudd S.M., Graf E.L.S., Maçenco L.C. 2021. Isolating lithologic versus tectonic signals of river profiles to test orogenic models for the Eastern and Southeastern Carpathians. *Journal of Geophysical Research: Earth Surface*, **126**(8):e2020JF005970. <https://doi.org/10.1029/2020JF005970>
- Gallagher K., Hawkesworth C.J., Mantovani M.S.M. 1995. Denudation, fission track analysis and the long-term evolution of passive margin topography: application to the southeast Brazilian margin. *Journal of South America Earth Sciences*, **8**(1):65-77. [https://doi.org/10.1016/0895-9811\(94\)00042-Z](https://doi.org/10.1016/0895-9811(94)00042-Z)
- Gallen S.F. 2018. Lithologic controls on landscape dynamics and aquatic species evolution in post-orogenic mountains. *Earth and Planetary Science Letters*, **493**:150-160. <https://doi.org/10.1016/j.epsl.2018.04.029>
- Gallen S.F., Thigpen J.R. 2018. Lithologic controls on focused erosion and intraplate earthquakes in the eastern Tennessee seismic zone. *Geophysical Research Letters*, **45**(18):9569-9578. <https://doi.org/10.1029/2018GL079157>
- Gomes C.H. 2011. *História Térmica das regiões sul e sudeste da América do Sul: implicações na compartimentação geotectônica do Gondwana*. PhD Thesis, Universidade Federal do Rio Grande do Sul, Porto Alegre, 160 p.
- Guo C., Montgomery D.R., Zhang Y., Zhong N., Fan C., Wu R., Yang Z., Ding Y., Jin J., Yan Y. 2020. Evidence for repeated failure of the giant Yigong landslide on the edge of the Tibetan Plateau. *Scientific Reports*, **10**:14371. <https://doi.org/10.1038/s41598-020-71335-w>
- Hackspacher P.C., Godoy D.F., Ribeiro L.F.B., Hadler Neto J.C., Franco A.O.B. 2007. Modelagem térmica e geomorfologia da borda sul do Crátão do São Francisco: termocronologia por traços de fissão em apatita. *Revista Brasileira de Geociências*, **37**(4):928-938. <https://doi.org/10.25249/0375-7536.200737S47686>
- Hasui Y., Borges M.S., Morales N., Costa J.B.S., Bemerguy R.L., Jimenez-Rueda J.R. 2000. Intraplate neotectonics in South-East Brazil. In: International Geological Congress, 31., 2000, Rio de Janeiro. *Abstract...* Rio de Janeiro.
- Heilbron M., Mohriak W.U., Valeriano C.M., Milani E.J., Almeida J., Tupinambá M. 2000. From collision to extension: the roots of the southeastern continental margin of Brazil. In: Mohriak W.U., Talwani M. (Eds.). *Atlantic rifts and continental margins*. AGU Geophysical Monograph, **115**:1-32.
- Instituto Brasileiro de Geografia e Estatística (IBGE). 1991. *Cartas topográficas em 1:50.000 – Edição de 1991*. Available at: <http://loja.ibge.gov.br/cartas-mapas-e-cartogramas/mapeamento-topografico>. Accessed on: Feb. 30, 2015.
- Jenson S.K., Domingue J.O. 1988. Extracting topographic structure from digital elevation data for geographic information system analysis. *Photogrammetric Engineering and Remote Sensing*, **54**(11):1593-1600.
- Kirby E., Whipple K.X. 2001. Quantifying rock uplift-rates via stream profile analysis. *Geology*, **29**(5):415-418. [https://doi.org/10.1130/0091-7613\(2001\)029<0415:QDRURV>2.0.CO;2](https://doi.org/10.1130/0091-7613(2001)029<0415:QDRURV>2.0.CO;2)
- Kirby E., Whipple K.X. 2012. Expression of active tectonics in erosional landscapes. *Journal of Structural Geology*, **44**:54-75. <https://doi.org/10.1016/j.jsg.2012.07.009>
- Liu M., Stein S., Wang H. 2011. 2000 years of migrating earthquakes in North China: How earthquakes in midcontinents differ from those at plate boundaries. *Lithosphere*, **3**(2):128-132. <https://doi.org/10.1130/L129.1>
- Lopes A.E.V., Assumpção M., Nascimento A.F., Ferreira J.M., Menezes E.A.S., Barbosa J.R. 2010. Intraplate earthquake swarm in Belo Jardim, NE Brazil: reactivation of a major Neoproterozoic shear zone (Pernambuco lineament). *Geophysical Journal International*, **180**(3):1302-1312. <https://doi.org/10.1111/j.1365-246X.2009.04485.x>
- Mantovani M.S.M., Quintas M.C.L., Shukowsky W., Brito Neves B.B. 2005. Delimitation of the Paranapanema Proterozoic block: a geophysical contribution. *Episodes*, **28**(1):18-22.
- Marangoni Y.R., Mantovani M.S.M. 2013. Geophysical signatures of the alkaline intrusions bordering the Paraná Basin. *Journal of South American Earth Sciences*, **41**:83-98. <https://doi.org/10.1016/j.jsames.2012.08.004>
- Marques F.O., Nikolaeva K., Assumpção M., Gerya T.V., Bezerra F.H.R., Nascimento A.F., Ferreira J.M. 2013. Testing the influence of far-field topographic forcing on subduction initiation at a passive margin. *Tectonophysics*, **608**:517-524. <https://doi.org/10.1016/j.tecto.2013.08.035>
- Marques K.P.P., Santos M., Peifer D., Silva C.L., Vidal-Torrado P. 2021. Transient and relict landforms in a lithologically heterogeneous post-orogenic landscape in the intertropical belt (Alto Paranaíba region, Brazil). *Geomorphology*, **391**:107892. <https://doi.org/10.1016/j.geomorph.2021.107892>
- Maus S., Barckhausen U., Berkenbosch H., Bourmas N., Brozina J., Childers V., Dostale F., Fairhead J.D., Finn C., Von Frese R.R.B., Gaina C. 2009. EMAG2: A 2-arc min resolution Earth Magnetic Anomaly Grid compiled from satellite, airborne, and marine magnetic measurements. *Geochemistry, Geophysics, Geosystems*, **10**(8):Q08005. <https://doi.org/10.1029/2009GC002471>
- Menier D., Mathew M., Pubellier M., Sapin F., Delcaillau B., Siddiqui N., Ramkumar M., Santosh M. 2017. Landscape response to progressive tectonic and climatic forcing in NW Borneo: Implications for geological and geomorphic controls on flood hazard. *Scientific Reports*, **7**:457. <https://doi.org/10.1038/s41598-017-00620-y>
- Milani E.J., Melo J.H., Souza P.A., Fernandes L.A., França A.B. 2007. Bacia do Paraná. *Boletim de Geociências Petrobras*, **15**(2):265-287.
- Minerais do Paraná S.A. (MINEROPAR). 2005. *Cartas geológicas 1:250.000*. Available at: <https://www.iat.pr.gov.br/>. Accessed on: Feb. 15, 2015.
- Mohriak W.U., Nemcok M., Enciso G. 2008. South Atlantic divergent margin evolution: rift-border uplift and salt tectonics in the basins of SE Brazil. In: Pankhurst R.J., Trouw R.A.J., Brito Neves B.B., de Wit M.J. (Eds.). *West Gondwana pre-Cenozoic correlations across the South Atlantic region*. London: Geological Society, Special Publications, v. **294**, 1-8.
- Mooney W.D., Ritsema J., Hwang Y. 2012. Crustal seismicity and the earthquake catalog maximum moment magnitude (M<sub>cmax</sub>) in stable continental regions (SCRs): Correlation with the seismic velocity of the lithosphere. *Earth and Planetary Science Letters*, **357-358**:78-83. <https://doi.org/10.1016/j.epsl.2012.08.032>
- Morales N., Hasui Y., Borges M.S., Costa J.B.S., Jimenez-Rueda J.R., Bemerguy R. 2001. Intraplate Neotectonics in Southeastern Brazil. In: Uplift and erosion: driving processes and resulting forms – dynamics between crustal and surficial processes. Certosa de Portignano: INQUA / Neotectonics Commission e Ministero dell'Università e della Ricerca Scientifica. Abstracts..., p. 58.
- Moulin M., Aslanian D., Unternehr P. 2010. A new starting point for the south and equatorial Atlantic Ocean. *Earth-Science Reviews*, **98**(1-2):1-37. <https://doi.org/10.1016/j.earscirev.2009.08.001>
- Peate D.W. 1997. The Paraná-Etendeka Province. *Geophysical Monograph*, **100**:217-245. <https://doi.org/10.1029/GM100p0217>
- Peifer D., Persano C., Hurst M.D., Bishop P., Fabel D. 2021. Growing topography due to contrasting rock types in a tectonically dead landscape. *Earth Surface Dynamics*, **9**:167-181. <https://doi.org/10.5194/esurf-2020-68>
- Pérez-Peña J.V., Al-Awabdeh M., Azañón J.M., Galve J.P., Booth-Rea G., Notti D. 2017. SwathProfiler and NProfiler: Two new ArcGIS Add-ins for the automatic extraction of swath and normalized river profiles. *Computers & Geosciences*, **104**:135-150. <https://doi.org/10.1016/j.cageo.2016.08.008>
- Peyerl W.R.L., Salamuni E., Sanches E., Nascimento E.R., Santos J.S., Gimenez V.B., Silva C.L., Farias T.F.S. 2018. Reactivation of Taxaquara. Fault and its morphotectonic influence on the evolution of Jordão River catchment, Paraná, Brasil. *Brazilian Journal of Geology*, **48**(3):555-575. <https://doi.org/10.1590/2317-4889201820170110>
- Powell C.A., Thomas W.A. 2016. Grenville basement structure associated with the eastern Tennessee seismic zone, southeastern USA. *Geology*, **44**(1):39-42. <https://doi.org/10.1130/G37269.1>
- Quigley M., Sandiford M., Fifield K., Alimanovic A. 2007. Bedrock erosion and relief production in the northern Flinders Ranges, Australia. *Earth Surface Processes and Landforms*, **32**(6):929-944. <https://doi.org/10.1002/esp.1459>
- Reis A.M., Ma J.B.C., Seer H.J. 2020. Insights into tectonic reactivation and landscape development processes at the Paraná Basin border using integrated geomorphometric and radiometric analyses. *Brazilian Journal of Geology*, **50**(4):e20190018. <https://doi.org/10.1590/2317-4889202020190128>

- Riccomini C., Assumpção M. 1999. Quaternary tectonics in Brazil. *Episodes*, **22**(3):221-225. <https://doi.org/10.18814/epiugs/1999/v22i3/010>
- Riccomini C., Peggia A.U.G., Saloni J.C.L., Kohnke M.W., Figueira R.M. 1989. Neotectonic activity in the Serra do Mar rift system (southeastern Brazil). *Journal of South American Earth Sciences*, **2**(2):191-197. [https://doi.org/10.1016/0895-9811\(89\)90046-1](https://doi.org/10.1016/0895-9811(89)90046-1)
- Riccomini C., Sant'Anna L., Ferrari A. 2004. Evolução geológica do rift continental do sudeste do Brasil. In: Mantesso-Neto V., Bartorelli A., Carneiro C.D.R., Neves B.B.B. (Eds.). *Geologia do continente sul-americano: evolução da obra de Fernando Flávio Marques de Almeida*. São Paulo: Beca, p. 383-405.
- Riccomini, C., Velázquez, V.F., Gomes, C.B. 2005. Tectonic controls of the Mesozoic and Cenozoic alkaline magmatism in central-southeastern Brazilian Platform. In: Gomes C.B., Comin-Chiaromonte P. (Eds.). *Mesozoic to Cenozoic alkaline magmatism in the Brazilian Platform*. São Paulo: EDUSP-FAPESP, p. 31-55.
- Riffel S.B., Vasconcelos P.M., Carmo I.O., Farley K.A. 2015. Combined  $^{40}\text{Ar}/^{39}\text{Ar}$  and (U-Th)/He geochronological constraints on long-term landscape evolution of the Second Paraná Plateau and its ruiniform surface features, Paraná, Brazil. *Geomorphology*, **233**:52-63. <https://doi.org/10.1016/j.geomorph.2014.10.041>
- Saadi A., Machette M.N., Haller K.M. 2002. Map and database of quaternary faults and lineaments in Brazil. *USGS Open-File Report*, 02-230.
- Salamuni E., Edert H.D., Borges M.S., Hasui Y., Costa J.B.S., Salamuni R. 2003. Tectonics and sedimentation in the Curitiba Basin, South of Brazil. *Journal of the South America Earth Sciences*, **15**(8):901-910. [https://doi.org/10.1016/S0895-9811\(03\)00013-0](https://doi.org/10.1016/S0895-9811(03)00013-0)
- Salamuni E., Silva C.L., Nascimento E.R., Peyerl W.R.L., Farias T.F.S., Santos J.M., Moreira L.F., Gimenez V.B., Sanches E., Sowinski A.C.B. 2017. Fases de deformação Cenozoica no Sul do Brasil. In: Simpósio Sul Brasileiro de Geologia, 10., 2017, Curitiba. *Anais...*
- Santos J.M., Salamuni E., Silva C.L., Sanches E., Gimenez V.B., Nascimento E.R. 2019. Morphotectonics in the Central-East Region of South Brazil: Implications for Catchments of the Lava-Tudo and Pelotas Rivers, State of Santa Catarina. *Geomorphology*, **328**:138-156. <https://doi.org/10.1016/j.geomorph.2018.12.016>
- Santos M., Ladeira F.S.B., Batezelli A. 2019. Indicadores geomórficos aplicados à investigação de deformação tectônica: uma revisão. *Revista Brasileira de Geomorfologia*, **20**(2):287-316. <https://doi.org/10.20502/rbg.v20i2.1564>
- Schwanghart W., Scherler D. 2020. Divide mobility controls knickpoint migration on the Roan Plateau (Colorado, USA). *Geology*, **48**(7):698-702. <https://doi.org/10.1130/G47054.1>
- Seeber L., Gornitz V. 1983. River profiles along the Himalayas arc as indicators of active tectonic. *Tectonophysics*, **92**(4):335-367. [https://doi.org/10.1016/0040-1951\(83\)90201-9](https://doi.org/10.1016/0040-1951(83)90201-9)
- Silva R.M. 2021. *Influence of surface processes on post-rift faulting during divergent margins evolution*. PhD Thesis, Universidade de São Paulo, São Paulo, 131 p.
- Silva R.M., Sacek V. 2019. Shallow necking depth and differential denudation linked to post-rift continental reactivation: the origin of the Cenozoic basins in southeastern Brazil. *Terra Nova*, **31**(6):527-533. <https://doi.org/10.1111/ter.12423>
- Soares C.J., Guedes S., Jonckheere R., Hadler J.C., Passarella S.M., Dias A.N.C. 2016. Apatite fission-track analysis of Cretaceous alkaline rocks of Ponta Grossa and Alto Paranaíba Arches, Brazil. *Geological Journal*, **51**(5):805-810. <https://doi.org/10.1002/gj.2694>
- Stein S., Mazzotti S. 2007. *Continental intraplate earthquakes: science, hazard, and policy issues*. Geological Society of America, Special Paper 425, 402 p.
- Strugale M., Rostirolla S.P., Mancini F., Portela Filho C.V., Ferreira F.J.F., Freitas R.C. 2007. Structural framework and Mesozoic–Cenozoic evolution of Ponta Grossa Arch, Paraná Basin, southern Brazil. *Journal of South American Earth Sciences*, **24**(2-4):203-227. <https://doi.org/10.1016/j.james.2007.05.003>
- Swaney Z.A., Duebendorfer E.M., Fitzgerald P.G., McIntosh W.C. 2010. New core complex model for South Virgin-White Hills detachment and extension in the eastern Lake Mead area, southern Nevada and northwestern Arizona. Geological Society of America, Special Paper 463, 355-370. [https://doi.org/10.1130/2010.2463\(16\)](https://doi.org/10.1130/2010.2463(16))
- Szatmari P., Milani E.J. 1999. Microplate rotation in northeast Brazil during South Atlantic rifting: analogies with the Sinai microplate. *Geology*, **27**(12):1115-1118. [https://doi.org/10.1130/0091-7613\(1999\)027%3C1115:MRINBD%3E2.3.CO;2](https://doi.org/10.1130/0091-7613(1999)027%3C1115:MRINBD%3E2.3.CO;2)
- Talwani P. 2014. *Intraplate earthquakes*. New York: Cambridge University Press, 332 p.
- Talwani P. 2017. On the nature of intraplate earthquakes. *Journal of Seismology*, **21**:47-68. <https://doi.org/10.1007/s10950-016-9582-8>
- Telbisz T., Kovács G., Székely B., Szabó J. 2013. Topographic swath profile analysis: a generalization and sensitivity evaluation of a digital terrain analysis tool. *Zeitschrift für Geomorphologie*, **57**(4):485-513. <https://doi.org/10.1127/0372-8854/2013/01110>
- Tello Saenz C.A., Hackspacher P.C., Hadler Neto J.C., Iunes P.J., Guedes S., Ribeiro L.F.B., Paulo S.R. 2003. Recognition of Cretaceous, Paleocene, and Neogene tectonic reactivation through apatite fission-track analysis in Precambrian areas of southeast Brazil: association with the opening of the South Atlantic Ocean. *Journal of South American Earth Sciences*, **15**(7):765-774. [https://doi.org/10.1016/S0895-9811\(02\)00131-1](https://doi.org/10.1016/S0895-9811(02)00131-1)
- Tinós T.M., Ferreira M.V., Zaine J.E., Riedel P.S. 2014. Técnicas de visualização de modelos digitais de elevação para o reconhecimento de elementos de análise do relevo. *Geociências*, **33**(2):202-2015.
- Torsvik T.H., Rousse S., Labails C., Smethurst M.A. 2009. A new scheme for the opening of the South Atlantic Ocean and the dissection of an Aptian salt basin. *Geophysical Journal International*, **177**(3):1315-1333. <https://doi.org/10.1111/j.1365-246X.2009.04137.x>
- Tucker G.E., Whipple K.X. 2002. Topographic outcomes predicted by stream erosion models: Sensitivity analysis and intermodel comparison. *Journal of Geophysical Research*, **107**(B9):1-16. <https://doi.org/10.1029/2001JB000162>
- Vasconcelos D.L., Marques F.O., Nogueira F.C.C., Perez Y.A.R., Bezerra F.H.R., Stohler R.C., Souza J.A.B. 2021. Tectonic inversion assessed by integration of geological and geophysical data: The intracontinental Rio do Peixe Basin, NE Brazil. *Basin Research*, **33**(1):705-728. <https://doi.org/10.1111/bre.12491>
- Whipple K.X., Tucker G.E. 1999. Dynamics of the stream-power river incision model: Implications for height limits of mountain ranges, landscape response timescales, and research needs. *Journal of Geophysical Research*, **104**(B8):17661-17674. <https://doi.org/10.1029/1999JB900120>
- Whittaker A.C. 2012. How do landscapes record tectonics and climate? *Lithosphere*, **4**(2):160-164. <https://doi.org/10.1130/RF.L003.1>
- Whittaker A.C., Attal M., Allen P. 2010. Characterizing the origin, nature and fate of sediment exported from catchments perturbed by active tectonics. *Basin Research*, **22**(6):809-828. <https://doi.org/10.1111/j.1365-2117.2009.00447.x>
- Whittaker A.C., Cowie P.A., Attal M., Tucker G.E., Roberts G. 2007. Contrasting transient and steady-state rivers crossing active normal faults: new field observations from the Central Apennines, Italy. *Basin Research*, **19**(4):529-556. <https://doi.org/10.1111/j.1365-2117.2007.00337.x>
- Wobus C., Whipple K.X., Kirby E., Snyder N., Johnson J., Spyropolou K., Crosby B., Sheehan D. 2006. Tectonics from topography: procedures, promise and pitfalls. In: Willett S.D., Hovius N., Brandon M.T., Fisher D.M. (Eds.), *Tectonics, climate, and landscape evolution*. Geological Society of America Special Paper 398, Penrose Conference Series, pp. 55-74. <https://doi.org/10.1130/SPE398>
- Zalán P.V., Wolf S., Conceição J.C., Astolfi M.A.M., Vieira I.S., Appi C.T., Zanotto O.A., Marques A. 1991. Tectonics and sedimentation of the Paraná Basin. In: International Gondwana Symposium, 30., 1991, São Paulo. *Proceedings...* p. 83-117.
- Zoback M.L., Richardson R.M. 1996. Stress perturbation associated with the Amazonas and other ancient continental rifts. *Journal of Geophysical Research*, **101**(B3):5459-5475. <https://doi.org/10.1029/95JB03256>